AN ABSTRACT OF THE THESIS OF

Preston S. Gabel for the degree of Master of Science in Mechanical Engineering presented on April 25, 1996.

Title: Composite and Adhesive Technology Applied to Chain Saw Guide Bars

Abstract approved: Redacted for Privacy

Ernest G. Wolff

Increased competition in the market place for both occasional and professional chain saw users has led to a desire for improved performance in chain saw guide bars. One aspect of improved performance is lower bar weight. The primary focus of this research was to establish the feasibility of a lower weight, composite, chain saw guide bar.

A production steel chain saw guide bar was analyzed using COSMOS finite element modeling. This analysis determined the feasibility of totally or partially replacing the steel with a lower density composite material. Classical strength of materials analytical techniques for beams in bending were used to verify the FEA models accuracy. Additionally, strain gauges were used in high stress areas to further verify the FEA models.

Various fiber reinforced thermoplastic pre-pregs were considered for the prototype research. From the literature study performed, two candidate thermoplastic matrices were chosen for further evaluation.

Analyses of polyetherimide and polyphenylene sulfide were performed using differential scanning calorimetry and dynamic mechanical testing. From these tests, information concerning processing temperature and ultimate end use requirements were determined.

Necessary electric heaters and other apparatus were fabricated to produce composite lay-ups. Pre-preg fiber lay-up orientation was determined from the finite

element analysis and wear requirements. From the analysis and testing two prototype chain saw bars were designed and then fabricated.

The first bar was composed entirely of carbon reinforced polyetherimide. The second bar was a hybrid design utilizing steel side laminates adhesively bonded to a central core of carbon fiber reinforced polyphenylene sulfide. Fabricated prototype guide bars were evaluated using a production power head.

Composite and Adhesive Technology Applied to Chain Saw Guide Bars

by

Preston S. Gabel

A THESIS

submitted to

Oregon State University

in partial fulfillment of
the requirements for the
degree of

Master of Science

Completed April 25, 1996
Commencement June 1996

Master of Science thesis of Preston S. Gabel presented on April 25, 1996

APPROVED:

Redacted for Privacy

Major Professor, representing Mechanical Engineering

Redacted for Privacy

Head of Department of Mechanical Engineering

Redacted for Privacy

Dean of Graduate School

I understand that my thesis will become part of the permanent collection of Oregon State University libraries. My signature below authorizes release of my thesis to any reader upon request.

Redacted for Privacy

Preston S. Gabel, Author

ACKNOWLEDGMENTS

I would like to thank the many people who had an important role in making this work possible and encouraging it's timely completion. I would like to thank my wife Christy Gabel for the encouragement and support during this grand adventure. I would also like to give a special thanks to Dr. Ernest G. Wolff for help, guidance and support throughout my graduate education.

I would also like to acknowledge the loving support of my family especially my Mother and Father Carole and Rodman Gabel and my Parents-in-law Norma Jean and Steven Kearsley.

Thanks to the Oregon Cutting Systems Division of Blount Inc. for funding this research. I would also like to thank Rob Breitbarth, Jim Burrows and Iain Thomson for technical support and functioning as the corporate representatives.

To my graduate research committee, consisting of Dr. Jonathan Istok, Dr. Timothy Kennedy and Dr. Skip Rochefort, I offer my most sincere thanks.

A special thanks to Dr. Phillip Humphrey and Milo Clauson of the Forest Research Laboratory for use of their hydraulic press, material testing and technical assistance.

I would also like to thank the many people associated with Oregon State University who helped in small but important ways. I would especially like to thank Debbie Jimmerson, Suzanne Reininger, and DyAnn McVicker for going above and beyond the call of duty and always doing so with a smile.

TABLE OF CONTENTS

Page

TABLE OF CONTENTS (Continued)

Page

LIST OF TABLES

LIST OF ILLUSTRATIONS

LIST OF ILLUSTRATIONS (Continued)

Composite and Adhesive Technology Applied to Chain Saw Guide Bars

INTRODUCTION

Increased competition in the market place for both occasional and professional chain saw users has led to significant technological advances in power heads. Increased chain speed has resulted in improved cutting ability and substantial weight reduction. In this market, a weight difference of only a few ounces may give one power head advantage over the competitors.

Advances in bar technology, such as nose-sprockets and improved rail heat treating etc., have resulted in enhanced performance and greater user satisfaction. Unfortunately, improvements have been largely limited to decreased bar and chain wear. In relation to weight and vibration, chain saw bar technology has changed little over the years.

Improvements in materials technology and the markets' desire for enhanced product performance suggest that a switch to chain saw bars made of an engineered composite material be seriously considered. Fiber reinforced polymers and metals present significant potential improvements in strength/stiffness to weight ratios, vibration damping and corrosion resistance.

Description of a Chain Saw Guide Bar

A standard chain saw guide bar consists of three major structural regions: the power head mounting region, bar body and replaceable sprocket nose (RSN) see figure 1. The present construction material is a modified 5150 alloy steel. The yield strength for this

alloy is between 175 and 250 ksi depending on the hardness. Hardness of various regions of the bar is a function of the desired wear performance. For example the bar body is exposed to less wear and is primarily structural. As a result a higher degree of

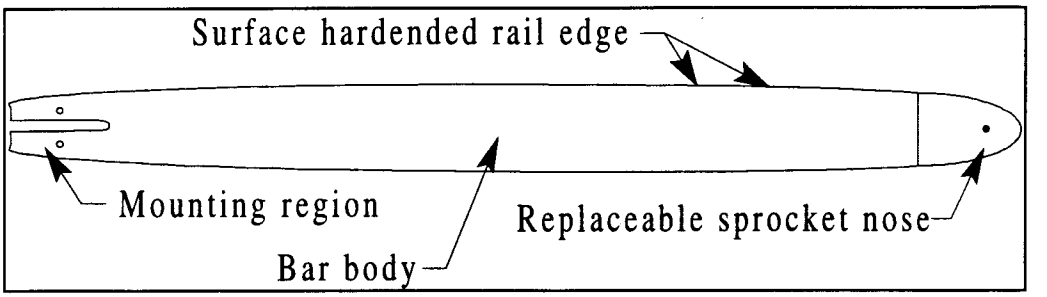

Figure 1. Major regions of a chain saw guide bar

toughness rather than hardness is desirable. In this region the bar is typically 38-44 Rockwell C (RC). The region sustaining the highest wear rate is the bar rail where the chain travels. A typical hardness for this region is 56-60 RC [1]. Hardness is modified by standard heat treatment procedures.

Carbon Fiber Reinforced Polymers as an Alternative to Steel

The available stiffnesses for carbon fibers range from approximately 20Msi to 130Msi compared to steels 30Msi. Carbon fibers are also relatively strong, typically around 200ksi or higher [2]. However, carbon-polymer composites are considerably less dense than steel. For example, steel has a density of 7.87g/cm3. Carbon-polymer composites typically have densities around 1.2g/cm3 which is roughly 1/7 that of steel [3].

In applications requiring less stiffness, while maintaining a significant weight reduction over steel, other composite materials such as fiber glass-polymer composites can

be utilized. Glass composites tend to be slightly more dense than carbon composites (1.6g/cm3) and less stiff (2 Msi) but with significant cost savings over similar carbon reinforced composites [4].

Thermoplastics vs. Thermosets as a Matrix

Both thermoplastic and thermosetting materials were considered as candidate matrices in conjunction with the glass and carbon fibers. Each of these broad classes of polymers have general characteristics which should be considered when making material selection decisions.

Thermosets are typically cheaper than thermoplastics with similar properties. Thermosets typically have better dimensional stability due to their completely cross-linked structure. A completely cross-linked thermoset is structurally an enormous single molecule rather than a "loosely" bonded collection of shorter polymer chains as is the case for a thermoplastic. Some thermosets can also be processed at room temperature which makes special heaters unnecessary. Thermosetting polymers are relatively inert once the cross-linking process is complete. This can be an important feature where evaporation or outgassing of short polymer fragments or volatile chemicals is a concern.

Thermoplastics have several advantages over thermosets which ultimately led to their selection as the matrix material for this research project. One major advantage of thermoplastics over thermosets is ease of storage. Thermosets are typically maintained in sub-freezing temperatures (often 0°F is specified) to prevent cross-linking during storage. Thermoplastic matrix composites have no special storage requirements beyond typical good material handling such as cleanliness and damage prevention.

Thermoplastics are also favored over thermoset matrices for environmental reasons. The curing or cross-linking process necessary for thermosets releases various environmentally sensitive chemicals. These chemicals are not only a concern for the environment but can also present a hazard to employees due to long term repeated exposure. The full impact of these components is not known, however in these times of extreme scrutiny from government and private institutions any chemical release is to be taken seriously and if possible eliminated. Thermoplastics do not involve a cross-linking cure step. These materials are fully reacted and release only a minute amount of the remaining volatile chemicals during product formation. Any volatiles are remnants from the original polymer manufacturing process.

In the chain saw guide bar application, thermoplastics offer the possibility of being reformable after damage. It is conceivable that a damaged bar could be repaired by reheating and reflowing the matrix polymer. On the negative side, fracture of the reinforcing fiber would limit the strength of the repaired bar, making subsequent damage to this region more likely.

Several base resins were considered to have the necessary thermal and chemical resistance properties to be used as matrices. Among these polyphenylene sulfide and polyetherimide are currently produced as fiber reinforced prepregs.

Polyphenylene sulfide

Polyphenylene sulfide (PPS), manufactured by Phillips Petroleum Company under the trade name Ryton is a crystalline, aromatic polymer (see figure 2). PPS has found uses in a wide range of applications where durability, temperature and chemical resistance is

necessary. Some of the industrial applications include motor casings, electrical connectors, boiler sensors, fuel and emission sensors and alternator components[4].

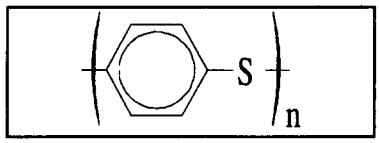

Figure 2. Chemical structure of polyphenylene sulfide (PPS).

Polyetherimide

Polyetherimide (PEI), like PPS is an aromatic polymer (see figure 3), however it is an amorphous material rather than crystalline. PEI is currently used in automotive and electrical applications where superior temperature and dimensional stability is required.

PEI as a neat resin, is one of the strongest engineering thermoplastics especially at elevated temperatures. For example, at 360°F the tensile strength is greater than 6 ksi and the flexural modulus in greater than 0.3 Msi[5].

Further data for PPS and PEI were collected in the course of this research project. Important details such as processing temperature and ultimate use temperature as well as some of the physical characteristics for these materials will be discussed in the following chapters.

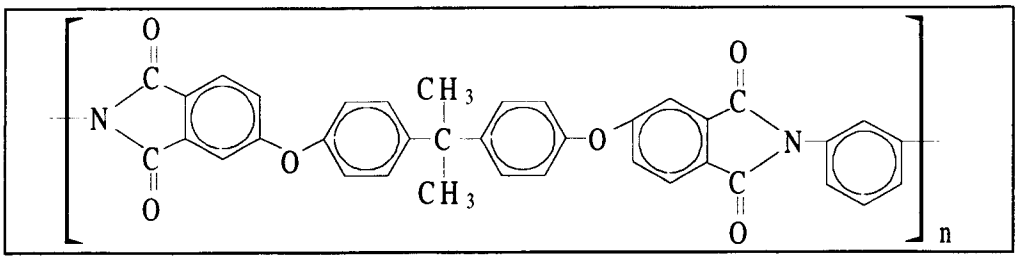

Figure 3. Chemical structure of polyetherimide

GENLAM and Classical Laminate Theory

GENLAM is a FORTRAN program used to calculate stiffnesses and strengths of thin laminated plates and sandwich structures. The code is based on laminated plate theory and takes into account anisotropy of individual laminae or plies. GENLAM was used to calculate the stresses within composite lay-ups due to external loading and shear stresses due to variations in the coefficient of thermal expansion (CTE).

Classical lamination theory (CLT) relates stresses to deformations and visa versa. CLT uses the characteristics of a single lamina and builds towards a complete structural laminate. The basic CLT theory can be expanded to include the stresses and strains due to temperature or moisture expansion coefficients.

Hooke's law extended to include orthotropic materials in principal material coordinates can be written as:

$$\begin{Bmatrix} \sigma_1 \\ \sigma_2 \\ \tau_{12} \end{Bmatrix} = \begin{vmatrix} Q_{11} & Q_{12} & Q_{16} \\ Q_{12} & Q_{22} & Q_{26} \\ Q_{16} & Q_{26} & Q_{66} \end{vmatrix} \times \begin{Bmatrix} \varepsilon_1 \\ \varepsilon_2 \\ \gamma_{12} \end{Bmatrix} \qquad (1)$$

The variables σ and $\tau 12$ are the stresses, ε and $\gamma 12$ are the strains and the Qij's are the material property engineering constants known as the reduced stiffnesses. This

equation can be transformed to any other in-plane coordinate system. The transformed equation is:

$$\begin{Bmatrix} \sigma_x \\ \sigma_y \\ \tau_{xy} \end{Bmatrix} = \begin{vmatrix} \overline{Q}_{11} & \overline{Q}_{12} & \overline{Q}_{16} \\ \overline{Q}_{12} & \overline{Q}_{22} & \overline{Q}_{26} \\ \overline{Q}_{16} & \overline{Q}_{26} & \overline{Q}_{66} \end{vmatrix} \times \begin{Bmatrix} \varepsilon_x \\ \varepsilon_y \\ \gamma_{xy} \end{Bmatrix} \tag{2}$$

The $\overline{Q}$ values in equation 2 are known as the transformed reduced stiffnesses. They represent the material properties in an arbitrary coordinate system [6]. Equation 2 can written in a more compact form and be specific to a particular lamina using the subscript k.

$$\{\sigma\}_k = [\overline{Q}]_k \{\varepsilon\}_k \tag{3}$$

The basic single lamina is expanded to form a complete laminate structure by making a few important assumptions. The interlaminar bonds are assumed to be complete and perfect. These bonds are also assumed to be infinitesimally thin, resulting in no shear deformation through the bond. Shearing strains in planes perpendicular to the middle surface are ignored in CLT. In conjunction with the shear assumption, the stresses perpendicular to the plane are also ignored. This collection of assumptions is known as the Kirchhoff hypothesis for plates.

The equation for the tensile and bending stresses a function of the tensile and bending strains is given without a complete derivation.

$$\{N\} = [A]\{\varepsilon_o\} + [B]\{k\}$$
$$\{M\} = [B]\{\varepsilon_o\} + [D]\{k\} \quad (4)$$

{N} are the stress resultants or stresses per unit width. {M} are the moment resultants due to bending. The values for ε_0 and k are the in-plane strains and curvatures of the laminate mid-plane, respectively. Equations 4 can be rewritten as the following single equation:

$$\begin{Bmatrix} N_i \\ M_i \end{Bmatrix} = \begin{vmatrix} A_{ij} & B_{ij} \\ B_{ij} & D_{ij} \end{vmatrix} \times \begin{Bmatrix} \varepsilon_o \\ k_j \end{Bmatrix} \quad (i,j = 1,2,6) \quad (5)$$

The matrix of values relating the strains and curvature to the stresses is known as the ABD matrix. Each of the components of this matrix represents a 3x3 matrix as the subscripts 1, 2 and 6 suggest. These subscripts represent the x, y and z directions respectively. The 3x3 A, B and D matrices are given by the following equations.

$$A_{ij} = \sum_{k=1}^{N} (\overline{Q}_{ij})_k (Z_k - Z_{k-1})$$
$$B_{ij} = \frac{1}{2} \sum_{k=1}^{N} (\overline{Q}_{ij})_k (Z_k^2 - Z_{k-1}^2) \quad (6)$$
$$D_{ij} = \frac{1}{3} \sum_{k=1}^{N} (\overline{Q}_{ij})_k (Z_k^3 - Z_{k-1}^3)$$

The subscript k represents the individual lamina and z is the perpendicular distance from the geometric mid plane of the entire laminate to the lamina surface (see figure 4). The $\overline{Q}_{ij}$'s are the transformed reduced stiffness values from equations 2 and 3 .

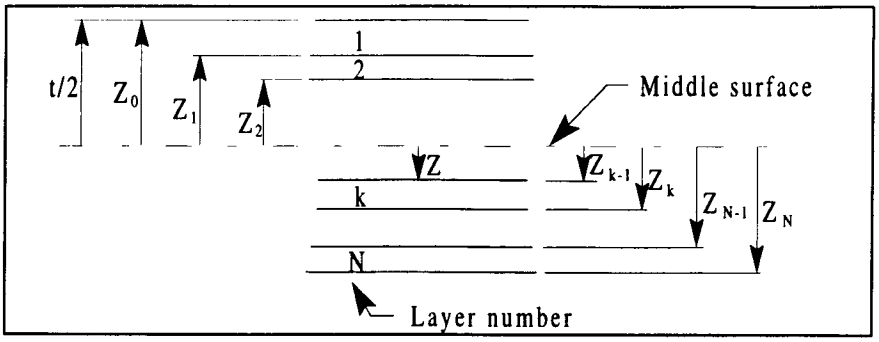

Figure 4. Geometry of an N-layered laminate

EXPERIMENTAL PROCEDURE

COSMOS Finite Element Modeling

The maximum stress and resultant deflection was determined using COSMOS finite element analysis (FEA) modeling. The FEA models were then verified using classical cantilever beam calculations. Regions of the guide bar where stresses were determined to be more critical were further verified using strain gauges where feasible.

The primary purpose of the FEA modeling was to gain some quantitative knowledge of the steel guide bar characteristics. Qualitatively, the steel bar is known to be "strong" as evidenced by an extremely low failure rate. In fact, structural failure during normal use is very rare. However, very little quantitative information is known. FEA and model verification data were used to establish some of the design and mechanical requirements for a composite guide bar.

FEA models were developed for the three critical regions of the bar; the tail and mounting region, the bar body and finally the replaceable sprocket nose (RSN) region. All models were evaluated with increasing mesh density until convergence was established.

The highest stresses from the cantilevered loads were found in the mounting region of the bar. Although the distance between the mounting studs is fixed, the bar can be moved forward or backward in the mounting slot to adjust chain tightness (see figure 5). It was discovered that certain adjustment positions resulted in significantly elevated stress conditions. Due to the higher stresses associated with the mounting region and the variability due to mounting position, several FEA models were created to better ascertain the stresses in this region.

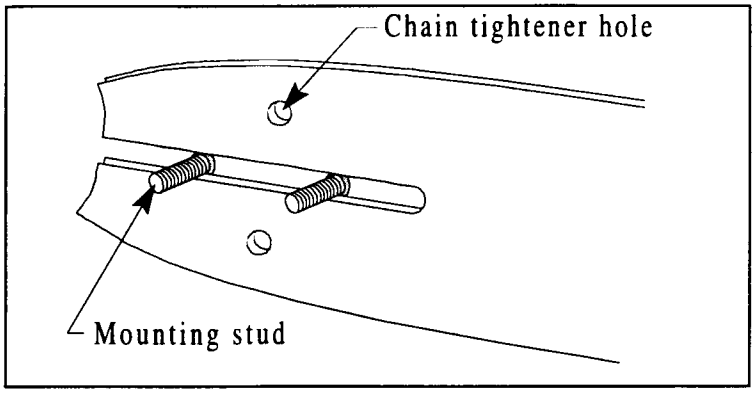

Figure 5. Mounting studs for attachment of saw bar to power head

The plots in the results section depict the von Mises stress for the given load, given by the equation:

$$\sigma' = \sqrt{\frac{(\sigma_1 - \sigma_2)^2 + (\sigma_2 - \sigma_3)^2 + (\sigma_1 - \sigma_3)^2}{2}} \tag{7}$$

For this equation the stresses σ_1 , σ_2 and σ_3 represent the stresses in the three orthogonal directions. Since all three stresses are included in the calculation of the von Mises stress, it represents the entire stress state at the point in question. In addition, this stress is used in the distortion energy failure criterion which states that yielding will occur when the von Mises stress exceeds the yield strength of the material. Although this failure theory is not directly applicable to composite design due to the anisotropic nature of composites, it does provide a good indication of the stresses imposed on the component.

FEA Model Verification with Classical Beam Theory

As mentioned, the FEA models were verified using classical cantilever beam theory. For purposes of evaluating the mounting region, the bar can be considered a cantilever beam with point loading at distance *l* (figure 6). The maximum stress for a cantilever

beam is at the top or bottom most "fiber." The basic equation which relates the load (P) to the stress (σ) is :

$$\sigma_{max} = \pm \frac{6Pl}{bh^2} \tag{8}$$

This equation was applied to the chain saw bar in both the vertical plane, as shown in figure 6, and in the horizontal plane i.e. load P on the face.

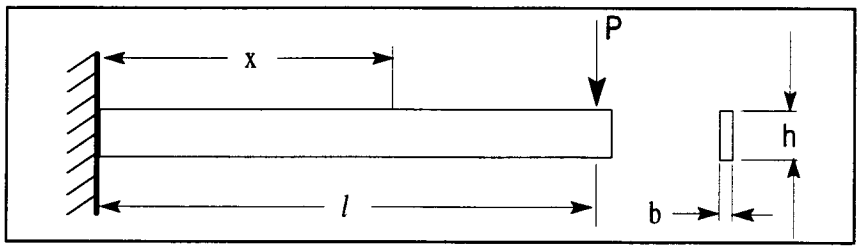

Figure 6. Diagram of classical beam assumption for chain saw guide bar

FEA Model Verification Using Strain Gauges

Strain gauges were utilized as a means of further verifying the COSMOS models. As the name suggests, strain gauges are designed to detect surface strains on a material to which they are adhesively mounted. They are essentially a length of wire for which the resistance is precisely known (often 350Ω). The wire is traced back and forth on the surface of a non-conducting material carrier, or matrix. The majority of the wire length runs along a single axis. The length of each pass of the wire is called the gauge length (figure 7). In addition, strain gauges have solder tabs to which a set of wires can be attached. These wires conduct electrical current from a bridge circuit to the strain gauge

and back to the bridge circuit. The resistance of the gauge increases in proportion to the amount of strain.

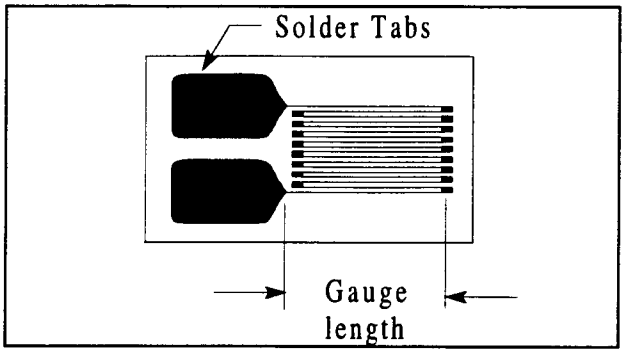

Figure 7. Diagram of basic strain gauge

By combining three gauges at angles to each other (45° or 120° depending on the type of gauge) near the point of interest, it is possible to resolve the principal strains and angle to the principal strain configuration on the surface of material being examined. Strain gauge manufactures often combine three gauges on a single matrix carrier using the appropriate orientation. This type of gauge is called a rosette. The equation which relates the principal strains to gauge strains for the 120° rosette gauges used on this project is:

$$\varepsilon_1,\varepsilon_2 = \frac{\varepsilon_0 + \varepsilon_{120} + \varepsilon_{240}}{3} \pm \sqrt{\frac{(2\varepsilon_0 - \varepsilon_{120} - \varepsilon_{240})^2}{9} + \frac{(\varepsilon_{120} - \varepsilon_{240})^2}{3}} \tag{9}$$

The rotation angle α from the strain gauge orientation to the principal strain orientation is found by the equation:

$$\tan(2\alpha) = \frac{\sqrt{3}(\varepsilon_{120} - \varepsilon_{240})}{2\varepsilon_0 - \varepsilon_{120} - \varepsilon_{240}} \tag{10}$$

When α is positive it is measured clockwise from the axis of the ε_0 strain gauge to the principal strain axis. Since steel is an isotropic material the stress is related to the strain by the Youngs modulus E according the to equation:

$$\sigma = E\varepsilon \tag{11}$$

Rosette gauges with 350Ω were acquired from Micro-Measurements Inc. The gauges were applied to one face of the bar as shown in figure 8. This position was

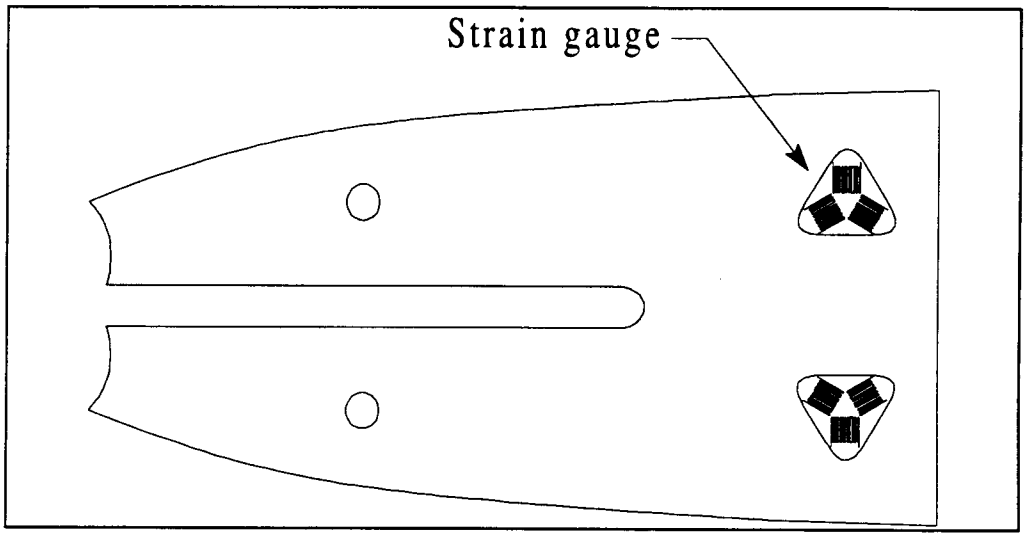

Figure 8. Position of resistance strain gauges

particularly good for resolving the stresses in out-of-plane bending i.e. a force on the side of the bar. Loads of 10 and 20 lbs were then applied in the out-of-plane configuration. The bar was also loaded to 44.75 lbs in-plane, that is to say, on the edge of the bar. For all these tests the load was applied at the tip of the bar to maximize the moment for the applied load.

Thermoplastic Characterization

Once the steel bar was characterized, the next requirement was to become familiar with the thermoplastic composite materials and the methods of processing them. Carbon fiber was the reinforcing material of first choice due to the steel like stiffness and the strength. However, the choice of which matrix material to use was not as clear cut. Polyphenylene sulfide (PPS), manufactured by Phillips Petroleum Company under the trade name Ryton, was considered a good candidate due to excellent chemical resistance and acceptable elevated temperature stability. Another candidate matrix material was polyetherimide (PEI) manufactured by General Electric under the trade name ULTEM. PEI has good chemical resistance and exceptional dimensional stability at elevated temperatures. In an effort to become more familiar with these materials several tests were performed to characterize their behavior.

Differential Scanning Calorimetry

The first test was differential scanning calorimetry (DSC). This test is widely used in industry to find the glass transition temperature (Tg), the melting temperature (Tm) and the heat of melting (Hm) of polymers. In addition, DSC testing can determine the heat of crystallization (Hc). If the Hc peak exists, the polymer is crystalline; if the peak is wholly absent the polymer is amorphous. Most polymers are not completely crystalline and will exhibit varying degrees of crystalline behavior. The area under the Hc curve is an indication of the degree of crystallinity for the polymer. These temperature related characteristics are important in processing the composite material into the final product. They are also important in predicting the performance of the polymer in the final application as a function of temperature.

The DSC measurements were performed on the Shimadzu Model DSC-50 operated by the Chemical Engineering Department at Oregon State University. For this test, an accurately weighed amount of each of the virgin polymers was placed in individual aluminum pans designed for this purpose. The pans were approximately 0.24 inches in diameter. Each pan was covered with an aluminum slip and placed in a small screw type press. When the screw lever was turned the anvil lowered over the pan and cover slip. The pan and slip edges were crimped shut to form a hermetically sealed unit. A third pan was prepared in the same manner lacking the polymer contents. This pan served as a stable measurement reference.

The DSC records variations in the heat to $1x10^{-5}$ mW. Due to this sensitivity the addition of skin oils from finger prints can negatively impact the test data. For this reason, care was taken throughout the pan preparation not to leave finger prints by touching either the polymer or the pans. To accomplish this, fairly deft use of tweezers was required.

To perform the measurements one of the pans containing the polymer in question and the empty pan are placed inside a small 1.5 inch diameter oven. Inside the oven were two small metal stages. Each stage was designed to serve as an electric heating element in addition to providing support for the aluminum pans. The stage area was then covered with a small metal lid and the oven itself was covered with a separate metal lid. Finally, an insulating cylinder was placed over the entire oven and a locking ring engaged to secure the system. This insulated cylinder helped provide a more stable temperature environment during the measurement process. It also served to contain cooling liquid nitrogen during the quench stage of testing. Pertinent data, such as polymer mass, pan design, temperature scan range and scan rate were then entered into controlling computer.

Once the measurement process began the DSC raised the temperature of the two stages and their respective pans at a constant rate. For this project the heating rate was set at 10°C/min up to the maximum temperature of 325°C for the PPS and 450°C for the

PEI. The amount of energy required to hold the temperature increase rate constant was recorded by the computer as a function of temperature. When temperature and energy were plotted against each other, the resultant curve contained many of the important temperature related polymer parameters. Various data analysis techniques, including linear regression and integration, were then employed on the computer to ascertain specific values such as Tg, Tm, Hm etc..

The next step in the DSC process involved cooling the pans back to room temperature. This was done by either quenching the sample with liquid nitrogen or allowing the pans to cool slowly, ≅7°C/min. In crystalline polymers the cooling rate partially determines the degree of crystallinity. Since information for both the amorphous and crystalline forms of the polymers was desired several runs employing both cooling techniques were performed.

Finally, the DSC curves were plotted with the Tg, Tm, Hc and Hm etc. labeled.

Dynamic Mechanical Testing

In order to further characterize the polymer matrices, dynamic mechanical testing was performed. The elastic and viscous properties of materials are important in predicting the vibrational characteristics and the response to repeated deformation. In addition, the elastic and viscous properties are largely a function of temperature. Determining these properties at various temperatures provides information about appropriate end use and processing temperature requirements.

Due to the fundamentally different responses of elastic and viscous properties of a polymer it is possible to separate these components through dynamic loading. The elastic component of the polymer varies linearly with strain and is thus, in phase with the load. For a sinusoidal load the stress τ is related to the load by the following equation.

$$\tau = G\gamma' \sin \omega t \tag{12}$$

where G is the shear stiffness, ω is the angular frequency and γ' is the strain amplitude.

In contrast, a purely viscous material acts like a linear dashpot. The stress is proportional to the rate of strain ($d\gamma/dt$). For a sinusoidally loaded dashpot the stress can be written as:

$$\tau = \eta\, \omega\, \gamma' \cos(\omega t) \tag{13}$$

where η is the viscosity.

From these equations it can be seen that the elastic and viscous components of the stress are out of phase. This phase difference is denoted by δ. For purely elastic materials δ is 0°. For purely viscous materials δ is 90°. For viscoelastic materials, such as thermoplastics, δ lies somewhere between these two extremes.

The in phase and out of phase components of the dependent variables related to the material properties are typically separated. The elastic in phase component variables are denoted by a prime. The viscous out of phase component variables are denoted by a double prime. Using this notation, the following relations for the storage modulus (G') and the loss modulus (G") can be defined.

$$G' \equiv \frac{\tau'}{\gamma'} \tag{14}$$

$$G'' \equiv \frac{\tau''}{\gamma''} \tag{15}$$

For these tests, two unidirectional lay-ups were fabricated from the PPS and PEI pre-pregs. In order to obtain the highest stiffness, the fibers were oriented in the longitudinal direction. Each sample was 12.13 mm wide and 48 mm long. The thicknesses for the PPS and PEI samples were 0.44 mm and 0.66 mm respectively.

The dynamic mechanical tests were performed on a Rheometrics RSA-II solids analyzer owned and operated by the Forest Research Laboratory at Oregon State University. The analyzer used a precision three point bend test apparatus in a temperature controlled cell. The composite samples were subjected to a sinusoidally varying load of ± 5 grams with a mean amplitude of 25 grams. The sinusoidal load frequency was set at 16.67 Hz for all dynamic tests. The temperature was swept from room temperature to 370°C (698°F) in 5°C (9°F) increments. At each increment the temperature in the cell was allowed to stabilize and then held an additional 90 seconds before the sinusoidal load was applied.

It is known that the elastic and storage moduli are frequency dependant. The "static" elastic and loss moduli can be obtained by extrapolating the data from multiple dynamic mechanical tests performed at many frequencies. In general, this extra testing is not performed unless the increase in precision is deemed to be worth the extra expense of time and money.

The applied load and the resultant force on the specimen stage was used by the analyzer to determine G' and G". In addition to the storage and loss moduli, the analysis program outputs the tangent of the phase difference (tanδ). The logs of these values were then plotted against temperature.

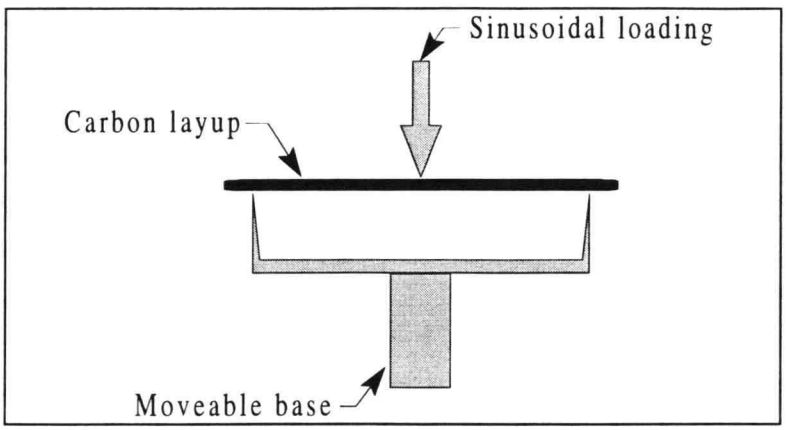

Figure 9. Dynamic three point bend apparatus

Lab Heater Fabrication

Two small high temperature heaters were built to efficiently produce sample coupons needed for testing. These heat units utilized mica dielectric heaters made by Minco Products Inc. Shortened development time, guaranteed heating capacity and assured even heating were the advantage of using off the shelf heating elements. These heaters are rated at 11 amps capacity at 32.7 Ω. The 6 inch round elements were backed with a quartz fiber insulating mat approximately 1/16 inch thick. An aluminum heat sink and backing plate were then constructed (see figure 10). The heaters can withstand temperatures to 1100°F. Due to the high temperatures attainable with these heating elements, constant pressure must be maintained as the organic binder in the mica degrades. The heater would literally fall apart without external support in the absence of the binder. Aside from structural support the aluminum heat sink also contributed to even heating across the platen.

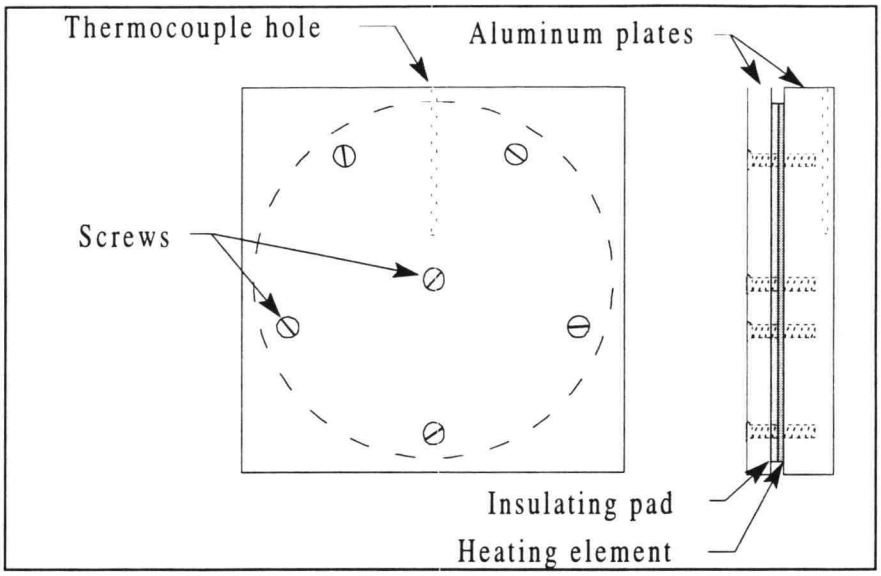

Figure 10. Diagram of small aluminum heater

Two 110 volt variacs were used to supply the current to the heaters. These instruments allowed complete adjustment over the full range of voltage from 0 volts to the maximum of 280 volts. Due to the potential for electrocution, extreme care was taken when using these devices.

Pre-pregs Familiarization Lay-ups

Once the heaters were completed, thermoplastic lay-up fabrication was begun. Ten Cate Advanced Composites bv, the manufacturer of both PEI and PPS pre-pregs suggested a consolidation temperature of 600°F for 15 minutes. They also suggested that 30 psi should be maintained during the heating process. After reaching 600°F the pressure should be ramped to 275psi during consolidation and maintained until the composite was cooled well below the glass transition temperature. These general procedures were followed throughout the research. A small 6 inch x 8 inch, 12 ton capacity press was used for imposing the desired pressure during consolidation.

Table 1. Steps required to fabricate a composite component using PEI or PPS matrix pre-pregs.

1. Design the lay-up fiber angles
2. Cut the pre-preg according to the fiber direction and shape desired
3. Stack the pre-preg cutouts per the fiber angle design
4. Add heavy duty aluminum foil to the top and bottom surfaces as a release sheet
5. Place the composite lay-up and aluminum release sheet in the heater platens without misalignment of the fiber orientation in the lay-up.
6. Place the heater and composite assembly in the press with woven quartz fiber mat insulation
7. Apply 25 psi and heat to processing temperature of 600°F (typically required 10 min.)
8. Once the processing temperature is reached increase pressure to 275 psi and hold for 15 min.
9. Cool the composite below the Tg before relieving the pressure
10. Remove the aluminum foil release sheet from the composite

Table 1 contains a concise list of steps required to generate a lay-up using the thermoplastic composite pre-pregs. Regardless of the size or end purpose, whether testing or making prototypes, these basic steps were followed.

As noted in step 4, aluminum foil was used as release sheeting rather than Teflon or silicone spray release products. The elevated temperatures reached during consolidation promote diffusion of these common release agents into the thermoplastic composite surface. These "slick" materials act as contaminates and are known to significantly degrade subsequent adhesive bonds [7].

The samples produced with this small heater apparatus were primarily used for establishing the proper fabrication technique. Test samples were also used for adhesive evaluations and tests with machining techniques. These issues will be discussed hereafter.

Adhesive Testing

Composite test samples of carbon/PEI and carbon/PPS were made using simple unidirectional lay-ups of 25 plies in the laboratory press and small heaters. Multidirectional structural requirements were minimal since the samples were used only for adhesive testing. For this reason the lay-ups were kept simple. The larger 4 x 4 inch composite plates were cut into four sample coupons of equal size (approximately 2 x 2 inches). These samples were lightly abraded with #200 grit silicon carbide sandpaper.

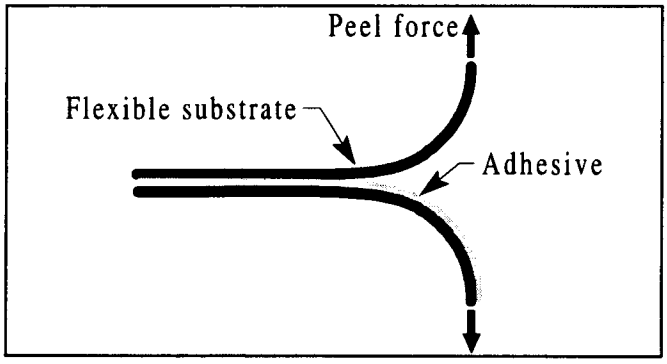

Figure 11. Peel failure of adhesive bond

Water was used to disperse the carbon/plastic dust particles. Isopropyl alcohol was used for cleaning and degreasing the abraded surfaces. The cleaning step is very important to assure a good bond. Skin oils from finger prints or other contaminants can greatly reduce the bond quality. A thin layer of the appropriate adhesive was applied to both surfaces of the composite coupons. The coupons were then pressed together to assure a complete bond between the surfaces. This was repeated for the various adhesive systems under scrutiny. The bonded coupons were then set aside for 48 hours to assure complete cure of the adhesive.

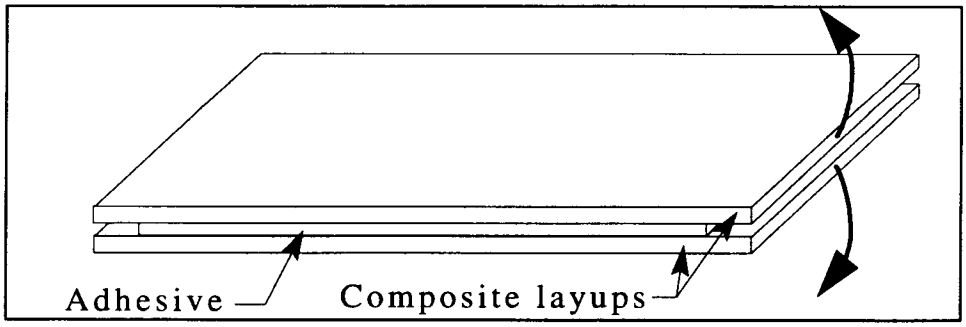

Figure 12. Adhesive cleavage test

Peel strength is an often reported in adhesive manufacturer data sheets. Peel implies that the substrate material flexes away from the adhesive bond during failure (see figure 11). Due to the extremely stiff nature of the carbon composites a more appropriate characteristic is the cleavage strength. Unfortunately cleavage data was not provided by the adhesive manufacturers. For this reason a simple test was developed to simulate a cleavage type failure with composite sample coupons and the various adhesives. These tests were designed to be qualitative rather than quantitative. As such, the strength of the bonds were judged in relation to the other adhesive bonds. The adhesively bonded composite coupons were forced apart at the adhesive gap toward one end (see figure 12). The bonds were evaluated on the force required to begin the cleavage failure and the amount of force required to continue that failure along the bond line. Table 2 contains a list of the adhesive systems evaluated and the respective manufacturers.

In addition to the adhesive systems mentioned in table 2, the bonding ability of the thermoplastic to steel was evaluated. Rather than use an adhesive, the pre-preg was consolidated, at normal temperature and pressure, between two prepared steel coupons. These samples were then evaluated on the same basis as the adhesively bonded test samples. This non-adhesive bond technique was utilized in the production of a small

prototype bar with steel side laminates and a central composite core. The fabrication of this prototype bar will be discussed at some length later in this chapter.

Table 2. Adhesive systems evaluated for cleavage properties.

Product	Adhesive Type	Manufacture
DP460	2 part epoxy	3M
DP805	2 part acrylic	3M
2043	2 part epoxy	Ciba Geigy
2214 high temp	1 part epoxy	3M
2042	2 part epoxy	Ciba Geigy
DP 420	2 part epoxy	3M

Composite Machining

It was realized that machining techniques such as milling and cutting would be necessary in the fabrication of a prototype guide bar. For this reason sample coupons were produced for the purpose of testing the various manufacturing techniques. Composite manufacturers often use special machining tools, such as diamond impregnated cutters or burrs. However, due to the limited production requirements and an effort to minimize cost, standard tools were utilized for these tests.

A cut off saw was used extensively where straight cuts were required. This tool was often used to produce smaller adhesive coupons from the larger lay-ups. The band saw was used on several occasions where curved cuts were necessary. In addition to the cutting, several standard machining techniques were tested. A 1/4 inch end mill was used

in an attempt to modify the surface of a lay-up. A 3/16 in slitting saw was used to evaluate cutting the composite edge to produce the chain saw bar guide rails.

Prototype Heater Fabrication

In order to manufacture full size components for prototype guide bars, considerably larger heater platens were required. Due to dimensional requirements it was determined that full size prototype heaters would be fabricated rather than purchased. These heaters utilized nichrome wire as heating elements. Due to the extremely high temperatures, attainable with nichrome wire, it was determined that quartz tubing should be used for electrical insulation rather than common glass tubing which might have melted. The

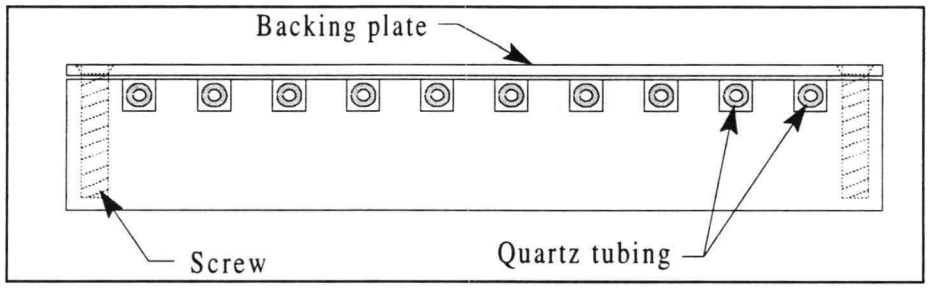

Figure 13. Side view of prototype heater

heater frame was fabricated from a 1/2 inch aluminum plate which was cut to 4 x 40 inches to accommodate the professional size guide bars. Grooves were cut into the plate on one face into which the insulated nichrome wire was inlaid (see figure 13). The relatively thick, aluminum plate provided the necessary support for the nichrome wire assembly and allowed the wire groves to be sufficiently deep. The thickness and the good thermal conductive properties of aluminum plate provided even heat distribution across

the face of the platen despite the high temperatures immediately around the nichrome wires

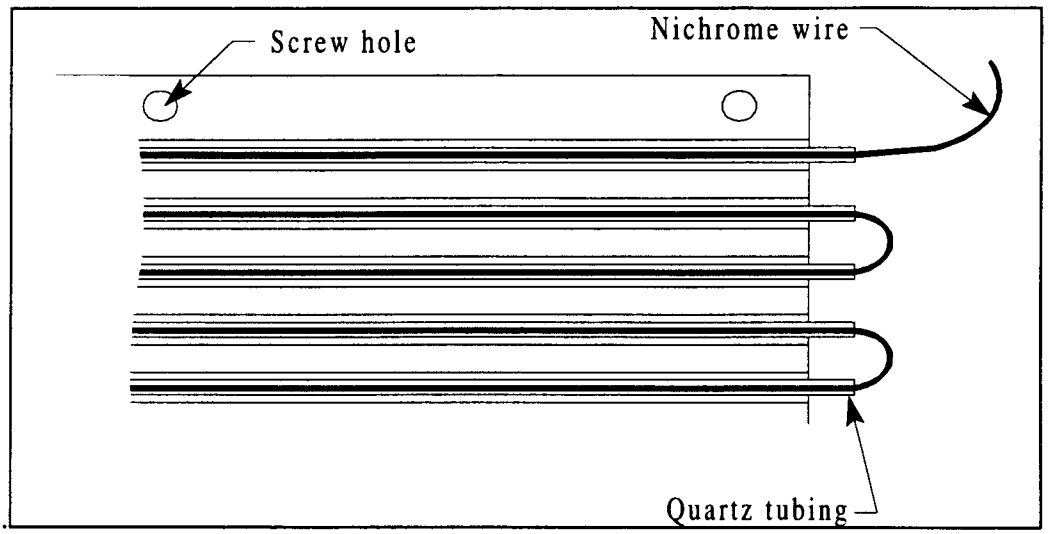

Figure 14. Detail of prototype heater end without backing plate.

The original design called for the wire ends to be enclosed within the aluminum frame. However, in the course or fabricating the heater it became apparent that the tight radii, required to implement this design, were not feasible. Furthermore, complete separation of the nichrome wire and the aluminum frame could not be assured at the wire bends due to the tight radii. This posed a potential safety risk due to electric shock. For these reasons it was determined that the nichrome wires would be allowed to extend beyond the aluminum frame and be completely exposed as shown in figure 14. Due to the wire ends being exposed, care was taken when using the heaters to prevent electrical shorts or potential electric shock.

When using the heaters an electrical connection block was used to connect the nichrome wire to the voltage source. As with the smaller coupon heaters, two 110 volt variacs were used to supply the current to the prototype heaters.

Non-adhesively Bonded Hybrid Guide Bar

With the preliminary work and equipment setup complete, the project took on two important directions. As originally proposed, an all composite bar was to be fabricated. In addition, it was determined that a hybrid bar should be developed that would incorporate steel side laminates with a central composite core (see figure 15). This hybrid composite bar would be significantly lighter than the all steel construction, while maintaining the exceptional durability and wear performance of the alloy steel. This design also offered lower material cost since a wide range of structural composite materials could be utilized in the low stress region of the core.

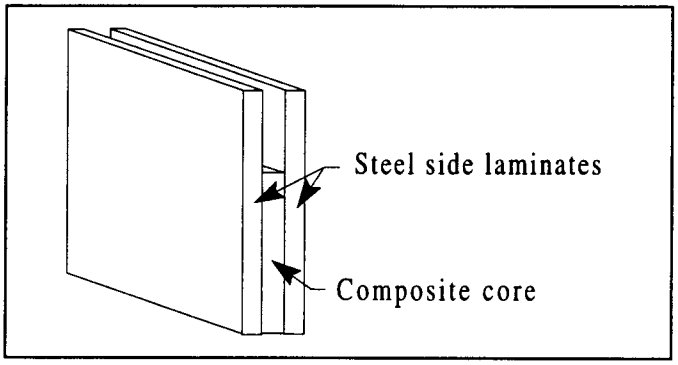

Figure 15. Cut out view of hybrid steel/ composite guide bar.

The first hybrid design utilized side laminates from the production version of a 24 inch guide bar. A central unidirectional PPS/carbon core was fabricated by using the steel core, which is normally spot welded to the side laminates, as a template. The pre-preg laminae were then cut individually with a razor knife to the appropriate shape. The laminae were then tacked together, in spot weld fashion, using an electric soldering iron. This tacking technique was very useful for maintaining proper fiber alignment when making multi-layered structures.

In an effort to maximize the thermoplastic to steel bond strength, the steel side laminates were treated with EC-3901 structural adhesive primer, manufactured by 3M. This primer is claimed to improve adhesion to metal surfaces.

The unconsolidated composite core was then positioned between the primed steel laminates and placed in the prototype heaters. The lab press was again used to provide the consolidation pressure. As mentioned the lab press surface is approximately 6 inches in length. Due to the difference in the press size to the bar dimensions, two 3 inch steel box beams were placed in the press to distribute the pressure over the prototype heaters and ultimately over the 24 inch bar. The temperature was then elevated to the prescribed 600° F and the pressure was raised to 275 psi. After the 15 minute consolidation period the guide bar was allowed to gradually return to room temperature.

The non-adhesively bonded hybrid bar was analyzed using GENLAM classical laminate theory software. There was some concern for the bond line shear strength due to the large difference in coefficient of thermal expansion for the carbon thermoplastic and the steel outer laminates.

Adhesively Bonded Hybrid Bar

The next prototype bar produced was a laminated system, like the bar just described, but an adhesive was used to bond the central composite core to the side steel laminates. Internal bond line shear stresses could be minimized with the adhesive since bonding could be performed at room temperature rather than 600°F. These stresses tended to be quite large and promoted delamination between the composite and steel in the hybrid bar previously described .

The composite core was fabricated from 14 laminae of 0.005 inch PPS/carbon pre-preg. To maximize the stiffness in the longitudinal direction only 0° laminae were used. Each lamina was cut to a rectangular shape of 36 x 3 inches.

Although the lab press used for making small samples had sufficient load capacity the small surface area over which the pressure was distributed proved to be a problem. As described above, the 3 inch box beams helped distribute the pressure for the consolidation of the 24 inch hybrid bar. However, as the bar length was extended to 36 inches assuring even pressure distribution became a problem due to flexure in the beam In addition to beam flexure, the side of the beam that was toward the heater tended to get quite warm relative to the side away from the heater. Due to the uneven thermal expansion rates, the beam would deflect. This further aggravated the consolidation pressure problem. Due to these phenomenon the bar ends which protruded from the press, experienced significantly lower consolidation pressure. A larger press would alleviate both the flexure problem and the deflection due to uneven heating. The solution to this dilemma was found in the Forest Products research lab press. This press has a 800,000 lb capacity with a 3 foot square pressing area. The load capacity was far greater than what was required and the pressing area was perfect for the 36 inch guide bar.

As in the previous work the necessary heat was provided by the prototype heaters which were driven by two 280 volt variacs. The heaters were placed in the large press and the composite core was place between two pieces of heavy duty aluminum foil in the heaters. A woven quartz fiber mat insulation was used to minimize the thermal losses due to conduction into the large steel press faces. The core was pressed to a thickness of 0.064 inches. The temperature and pressure were raised and maintained in the same manner as previously explained.

The next step was to cut the composite core from the rectangular shape to the proper curved bar shape. This was done by tracing the outline of the core onto the composite blank with a pencil. The blank was then cut out along this line on a band saw. Due to the imperfections in cutting with the band saw the core was further trimmed using a belt sander.

The top and bottom surfaces of the core were abraded with 200 grit silicon carbide sand paper in preparation for bonding. The core was then cleaned several times with methyl alcohol to remove surface contaminants such as dust and grease. The bonding surfaces of the steel side laminates were also prepared for bonding. This was done by abrading the surfaces with a wire brush until all signs of oxidation had been removed. The steel was then wiped down with methyl alcohol. This step was repeated until no discoloration could be detected on the towelette. The cleaned steel surfaces were then treated with EC-3901 structural adhesive primer.

Three aluminum pins for aligning the composite core and steel laminates were then fabricated on a metal lathe. The pins were pressed into the two holes reserved for the chain tightener and an alignment hole near the replaceable sprocket nose. With these pins in place the three layers were relatively stable and could be moved as a unit without serious concern of causing misalignment.

The composite core and steel side laminates were then separated for the application of the adhesive. From the qualitative adhesive testing described earlier, DP805 manufactured by 3M was determined to be the best adhesive for this prototype. Unfortunately DP805 has a cure time of only 5 minutes and an effective pot life of only 45 seconds. Due to the speed at which the adhesive had to be applied and the laminates pressed together, extra care was taken to assure that the necessary equipment would be available and be ready to use quickly. The large press was again used to provide the pressure necessary to obtain a good bond. The adhesive was generously applied to both sides of the composite core and spread evenly with a wooden tongue depressor. The steel side laminates were then positioned using the aluminum guide pins for alignment. The bar was placed between two layers of heavy duty aluminum foil to protect the press platens from any excess adhesive. The bar and foil where then placed in the press and approximately 20 psi was applied. To be absolutely sure that the adhesive was fully cured the pressure was maintained for approximately one hour.

The cured hybrid bar was removed from the press and examined. In the area around the RSN and mounting region, a slight excess of adhesive was observed. Due to improper mating with the power head and the RSN, removal of this adhesive was required. This was accomplished by trimming the adhesive back with a sharp knife.

All Composite Bar Lay-up

With the hybrid bar complete, the effort turned to the all composite bar. As discussed some testing had been done to assure that the composite was machinable using normal shop techniques. From this work it was known that the bar rails could be machined into the edge of a solid composite blank using a slitting saw. The other option would have been to design a method whereby the rails could be formed into the bar at the

time of consolidation. Ultimately, the preformed rail method may be the preferred process for a production bar, however, the time to generate the required tooling was prohibitive. For this reason the more technically simple method of machining the bar rails was chosen.

With the rail complication solved the task became the relatively straight forward effort to make a solid lamination of thermoplastic composite of sufficient size. This bar would be fabricated from a solid consolidated rectangular composite lay-up. The original fiber lay-up was intended to optimize the bar for the applied stresses. However, after consulting the literature on wear associated with composites it was determined that a significant number of 90° laminae improved wear characteristics. Additionally, small test samples with unsymmetric lay-ups, produced very warped laminates.

For purposes of lay-up visualization the bar can be thought of as 3 laminates which are each 0.064 inches thick; two sides and a core. For the reasons explained above, symmetric lay-up with several 90° laminae was chosen for the side laminates. This lay-up would also carry most of the out-of-plane bending loads. For this reason, 0° fibers were placed as the outermost layers. The lay-up also included 45° laminae to carry torsional loads and help with wear. Given these criteria the following lay-up was devised for the side laminates:

$$[0_2,+45,-45,90_3,-45,+45,0_2]$$

In an effort to maximize the longitudinal stiffness, the core utilized a unidirectional lay-up of thirteen 0° lamina. The side laminates and the core were designed to be the same thickness (0.064 inches). However, due to the unidirectional fibers tendency to pack together tighter, or nest, two extra laminae were added to the core section. The complete lay-up with side laminates and the core was:

$$[0_2,+45,-45,90_3,-45,+45,0_{17},+45,-45,90_3,-45,+45,0_2]_T$$

A sample 4 inch by 4 inch coupon was fabricated using this lay-up in the lab press. From this test, the lay-ups curvature and machinability were confirmed. However, due to the greater thickness associated with this lay-up, there was considerably more material flow during consolidation. For thicker lay-ups, like the all composite bar consisting of 35 laminae, the ability to control the thickness while consolidating the lay-up at the appropriate pressure became a significant problem.

For very large lay-ups, like those in actual production, typically 4 by 8 feet or larger, the tendency for the composite to flow is minimal. For these large plates the material constrains itself in the plane. Any given point in the lay-up, away from the vicinity of the edges, behaves more like a small section of an infinitely large lay-up. Some motion is obviously expected, particularly near the edges of the lay-up. However, the perimeter is relatively insignificant in area compared to the sheet as a whole. In these large plates (the perimeter which might be out of specifications) is trimmed and discarded.

Due to the relatively short dimensions for the all composite bar (40 by 4 inches) the dimensional restraints of the large production panels could not be expected. As a result, maintaining the correct thickness over the entire composite blank proved to be challenging.

One suggested solution was to use shims. The shims would prevent the press from over squeezing the lay-up. This solution would have provided the necessary dimensional control but consolidation pressure could not be maintained as the lay-up reached the minimum thickness.

Consolidation Die Fabrication

A die was the chosen solution to the problem of maintaining consolidation pressure while containing the semi-fluid composite material. This die was constructed of a 5/8 aluminum plate with side walls made from 3/8 x 1/2 inch aluminum bar stock. As shown in figure 16, the side walls were attached to the plate with 1/4 inch flat head screws. The objective of this design was to provide the necessary containment, while allowing the die to be disassembled if necessary. The male portion of the die was a 4 by 39 inch piece of 1/4 inch aluminum plate. The male portion of the die fit into the die cavity with approximately 0.01 inch clearance on all sides. With the composite lay-up placed in the die cavity and the male pressure plated on top, the composite material was held captive under the consolidation pressure.

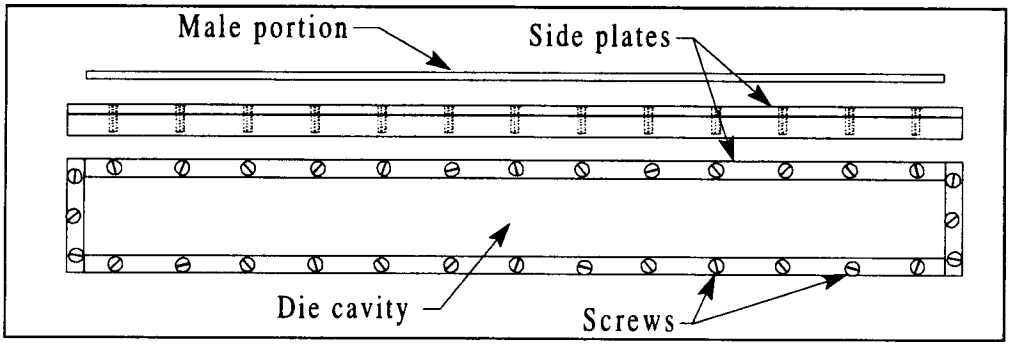

Figure 16. Composite fabrication die.

The individual PEI/carbon laminae were then cut to 40 x 4 inches with the fiber orientation according to the lay-up design discussed in the previous section. The individual laminae were placed in the die cavity and tacked together with a soldering iron. Tacking the laminae together assured proper fiber orientation was maintained since there were many pieces to make up the lay-up. The zero degree laminae could be cut into a

solid strip of material, however the 45's and 90's had to be cut and pieced together since the stock material was only 8 inches wide.

As in previous lay-ups, aluminum rather than Teflon release sheeting was used to facilitate removal of the composite bar from the tooling. Aluminum is preferred over Teflon type films with PEI and PPS due to the high temperatures attained during consolidation. At these temperatures the Teflon begins to melt and diffuses into the composite surface. Subsequent bonds to the composite surface are significantly degraded due to the diffused Teflon. For the all composite bar a thicker aluminum sheet (0.017 in) was used. This sheet was more resistant to tearing during removal from the composite blank.

The male pressure plate was then placed over the composite lay-up in the die cavity and the entire assembly was positioned between the two heaters in the large 800,000 lb press. Two inch strips of woven glass insulation were used to reduce the conductive losses of the heaters and die assembly to the steel press platens. As in all previous tests, the temperature was raised to the consolidation temperature of 600°F under 25 psi. Once 600°F was attained the pressure was raised to 300 psi. The composite was consolidated for 20 minutes and then the heaters were switched off.

After a couple hours the die and bar where cool enough to be removed from the press. Upon removal from the press it was immediately evident that the die was under tensile stresses sufficient to cause bowing. The cause of this stress will be discussed in the results section. The stresses were large enough to require the side plates of the die to be removed before the composite bar blank could be extracted from the die. In the process of removing the side plate, 8 screws were sheared off at the head leaving the studs in the aluminum die plate. The die side walls were pried over the unremoved studs, resulting in some damage to the aluminum sides. After much effort the composite bar blank was

removed from the die. The aluminum release sheet was then peeled from the composite blank.

Composite Bar Machining

Due to the complex curvature of the bar body and the need for a smooth surface upon which the chain can run, it was determined that water jet cutting the bar blank would be preferable to cutting on a band saw. The blank was taken to Pacific Laser Technologies in Beaverton Oregon to be cut. The tool path for the water jet was generated from an AUTOCAD DXF file.

Final machining, such as incorporating the replaceable sprocket nose adapter, rail guides and mounting region was performed by Oregon Cutting Systems (OCS) Division of Blount Inc. OCS has the necessary equipment, particularly computer numerical controlled (CNC) milling machines necessary for the curved cuts required to finish the bar. The RSN adapter would have been particularly difficult to fabricate without CNC equipment.

Guide Bar Testing

The hybrid composite chain saw guide bar was then tested by mounting it to a Husqvarna model 281XP power head with a loop of 3/8 inch pitch chain. The saw was used to cut logs varying in size from 2.5 inches to 26 inches in diameter. The saw/ bar combination was used for a single tank of gas.

The all composite bar was tested by Oregon Cutting Systems Division of Blount Inc. Several cuts were made in various sized logs to confirm the functionality of the all composite bar.

RESULTS AND DISCUSSION OF RESULTS

Finite Element Analysis (FEA)

The foundation of the design work was laid in the finite element modeling done to ascertain the strengths of the steel bar currently in production. Due to extremely low failure rates the steel bar was known to be"under stressed". Also due to the low failure rate, the need to understand the stresses imposed on the bar was minimal. The physical dimensions of the bar were a function of saw chain requirements rather than stress requirements. The finite element analysis (FEA) work provided the necessary information needed to establish the feasibility of a composite bar.

The guide bar was evaluated in the two primary bending loading configurations: in-plane (the configuration in normal use), and out-of-plane (accidental loading caused by tree pinching or levering). For the in-plane stress analysis a 50 lb was used. This corresponded to the test performed subsequently with strain gauges. It should be noted that this load is much higher than the static loads for normal use. A normal load for this configuration would be approximately 8 lbs at the nose of the bar.

For the out-of-plane loading 20 lbs was used. This configuration was also confirmed with actual tests performed with loads of 20 lbs.

In both the in-plane and out-of-plane cases the stress resultant can be adjusted for any given load due to the linearity of stress. This assumes that the load stays within the linear region of the stress strain curve. Pages 39 through 47 are the FEA stress plots.

The first analysis performed was for the out-of-plane loading case. For this test the load was placed at the nose of the bar 35 inches ahead of the power head mount. The mount was assumed to be a perfect fixture preventing all translation and rotation. Figure 17 depicts the peak stresses ahead of the power head. As expected, the stress varies down

the bar from the peak stress near the mount to the minimum stress at the point load (not shown). Variations from the linear stress distribution down length of the bar can be seen near the mounting slot where the stress actually decreases somewhat. The peak von Mises stress for this 20 lb bending load was approximately 50 ksi.

The most critical portion of the bar, in terms of the peak stress, was the mounting region. In this area the bending moments and the resultant stress reached their peak. Two configurations for bar mounting were determined to best model reality. The perfectly clamped bar was simulated by a line of nodal constraints that gave perfect translational and rotational restraint. The improperly mounted bar was modeled using only the mounting studs and the chain tightener for translational support. These points also prevented rotation about the Z-axis. For purposes of modeling the chain tightener node was used for the remaining X and Y-axis constraints.

Figure 18 is a von Mises stress plot for the peak stress area ahead of the power head mounting region. The mount is assumed to provide perfect support to the guide bar. This simulates a bar well clamped to the power head. The load used for this analysis was 50 lbs at the nose of the bar.

As expected, the maximum tensile and compressive loads can be seen at the top and bottom most point of the bar. The peak stress for this load was approximately 82 ksi.

The next two plots, figures 19 and 20 depict the stresses for the imperfectly supported guide bar. The bar depends totally on the mounting studs and the chain tightener pin for support. This simulates a totally free floating bar loosely fastened to the power head. Two bar positions, in relation to the mounting studs, were chosen for this analysis: extremely far forward and extremely far back. In reality the bar is adjusted to some point between these two extremes. The peak stress of 87 ksi was associated with the extremely far back mounting configuration. The stress was highly localized towards

the front of the mounting slot and the top of the bar. The peak stress for the far forward mounting configuration was 51 ksi.

The other critical region of the bar in terms of stress was the replaceable sprocket nose (RSN) web. The 0.066 inch web on the bar body is used to attach the RSN to the bar. The present design of the RSN is designed to fail before damage is sustained by the RSN web on the bar body.

Through testing, the failure of the RSN was determined to occur at a load of 43 lbs placed 35 inches from the RSN. The resultant failure moment was used in the FEA model to determine the stresses in the RSN web. Figure 21 depicts one half of the RSN mounting region of the guide bar. Symmetry permitted only half the region to be modeled, thus saving computer analysis time. From this figure the peak stress can be seen to be approximately 78 ksi.

Due to the simple loading and constraints for the previous plots the peak principal stress was easily determined by inspection. However, the loading and constraints of the RSN web were not as trivial. For this reason, σ_x and σ_y components of the stress were plotted in addition to the von Mises stress plot. Figures 21, 22 and 23 are the von Mises, σ_x and σ_y stress plots respectively. The maximum stress occurred in the X-direction with a value of approximately 58 ksi. The Y-direction peak was approximately 36 ksi.

Some extra FEA modeling was performed using a guide bar design that is now obsolete due to fatigue failures. This design incorporated a closed mounting slot rather than the open slot seen in the drawings and FEA plots. Fatigue failures occurred in the tail and chain tightener holes. The correlation of the fatigue failures to the stresses, determined in the FEA modeling, helped verify that the analytical analysis was a valid simulation of the actual guide bar.

Figure 24 depicts the stresses with the mounting studs towards the tail of the bar in the closed mounting slot. The stress peak is approximately 66 ksi through the closed tail.

Figure 25 depicts the stresses for the mounting studs moved forward with the rear stud beneath the upper most chain tightener hole. The peak stresses for this plot are at both ends of the mounting slot and under the tightener hole. Eliminating the closed tail obviously eliminated fatigue failure at this point. The interesting point is that this design change also relieves some of the stress associated with the rear mounting stud. This can be seen by comparing the closed mount stress plots with the previous mounting region plots.

This is more than an interesting side note; as mentioned earlier the correlation between the FEA stress analysis and the exhibited fatigue failures help verify that FEA models are valid. In addition to this evidence, classical beam theory and strain gauges were also used to verify the models as well as obtain data for the steel guide bar behavior.

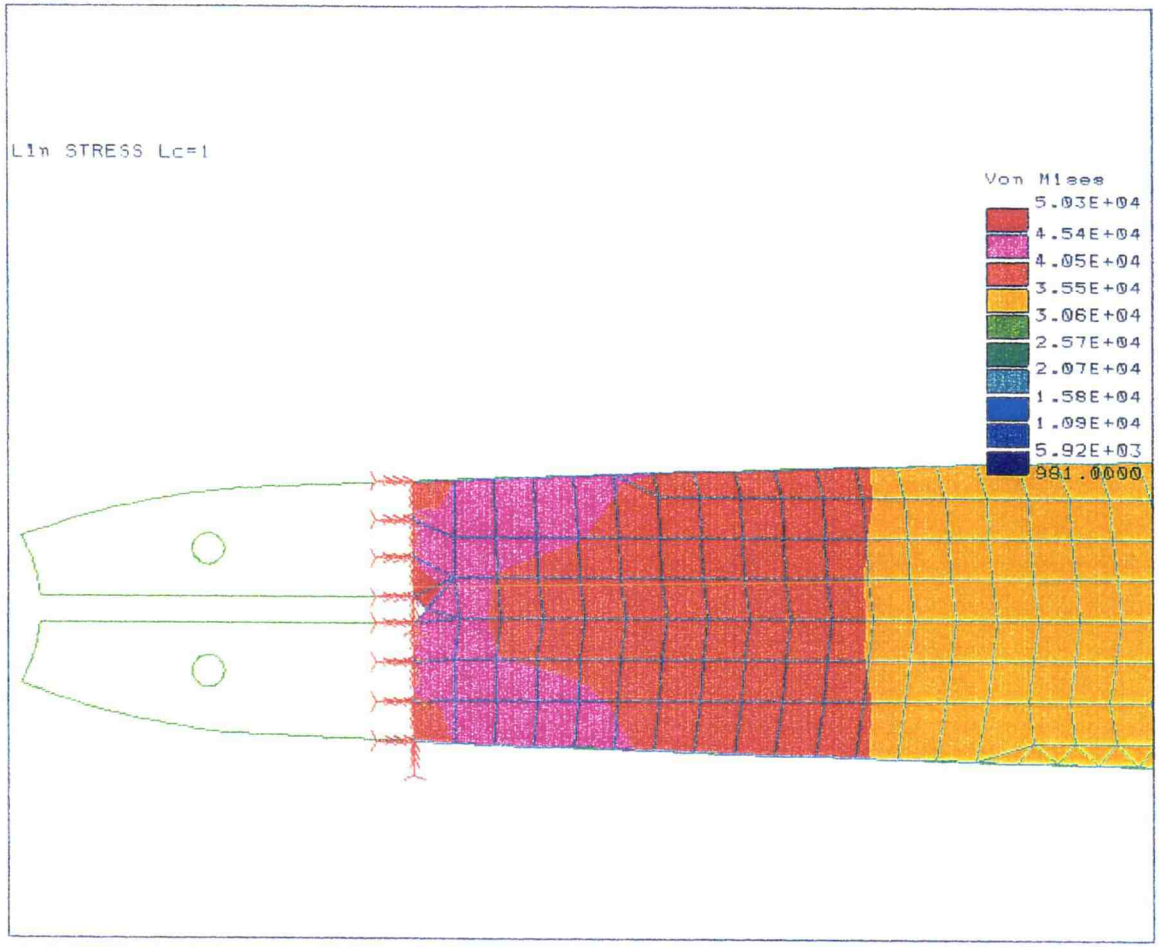

Figure 17. von Mises stress plot for guide bar with 20 lbs out-of-plane loading.

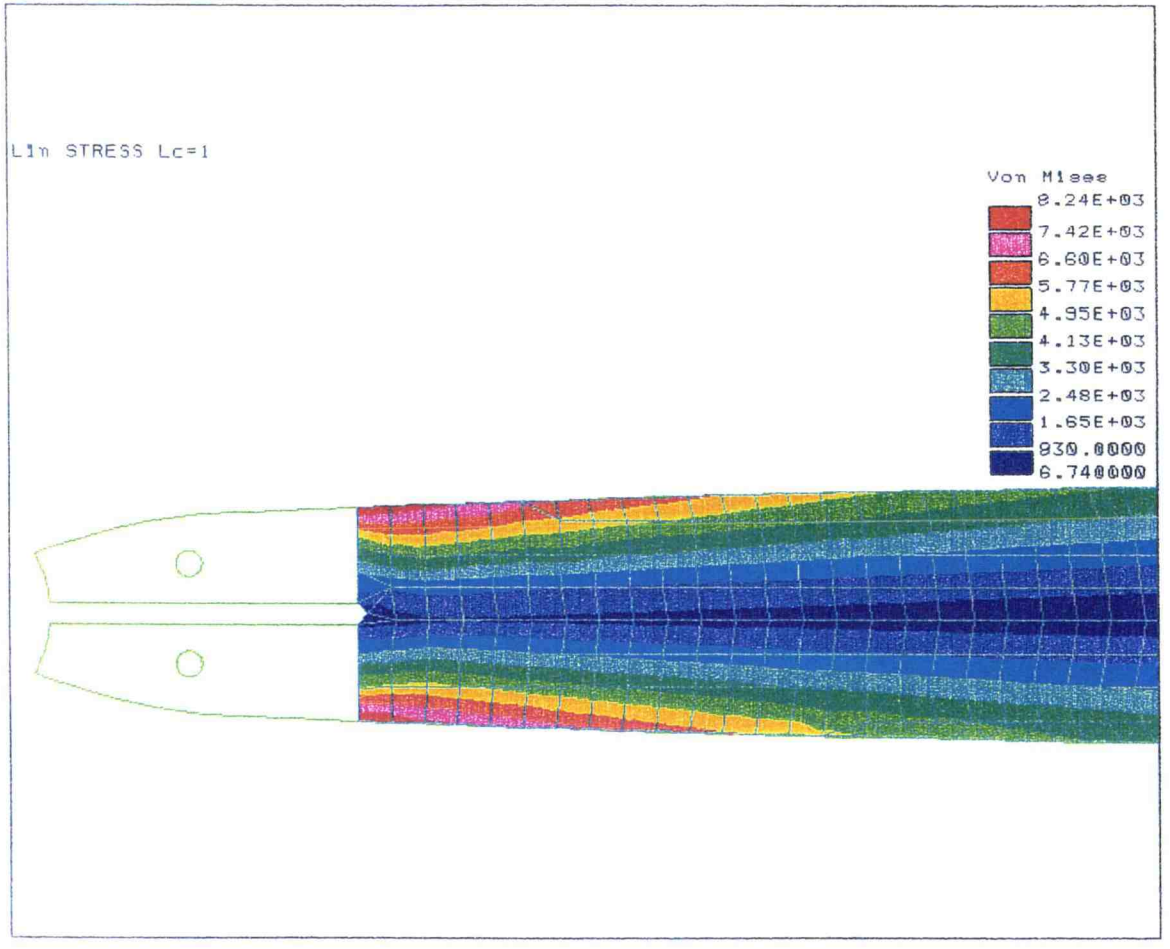

Figure 18. von Mises stress plot for 50lbs loaded in-plane with perfect restraint.

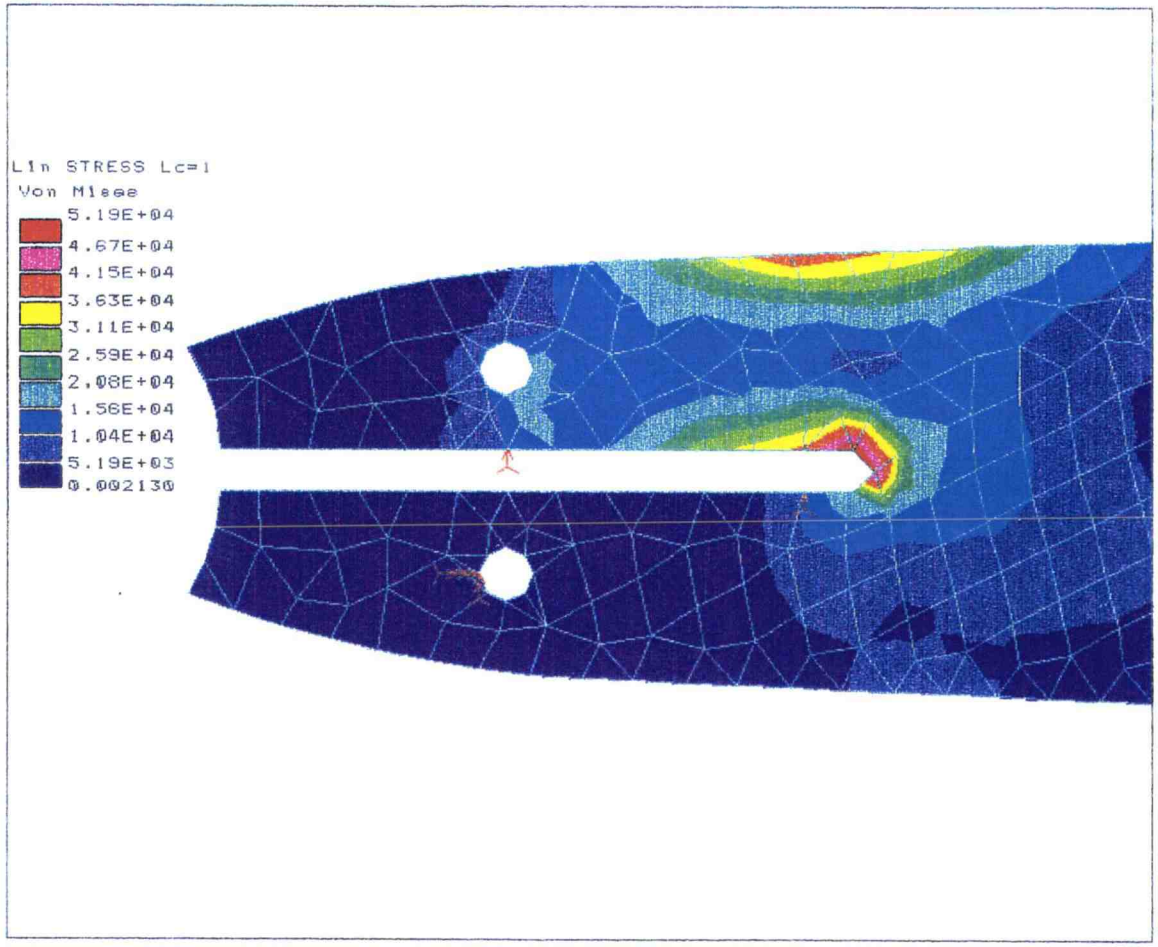

Figure 19. von Mises stress plot for pin supports near front of mounting slot.

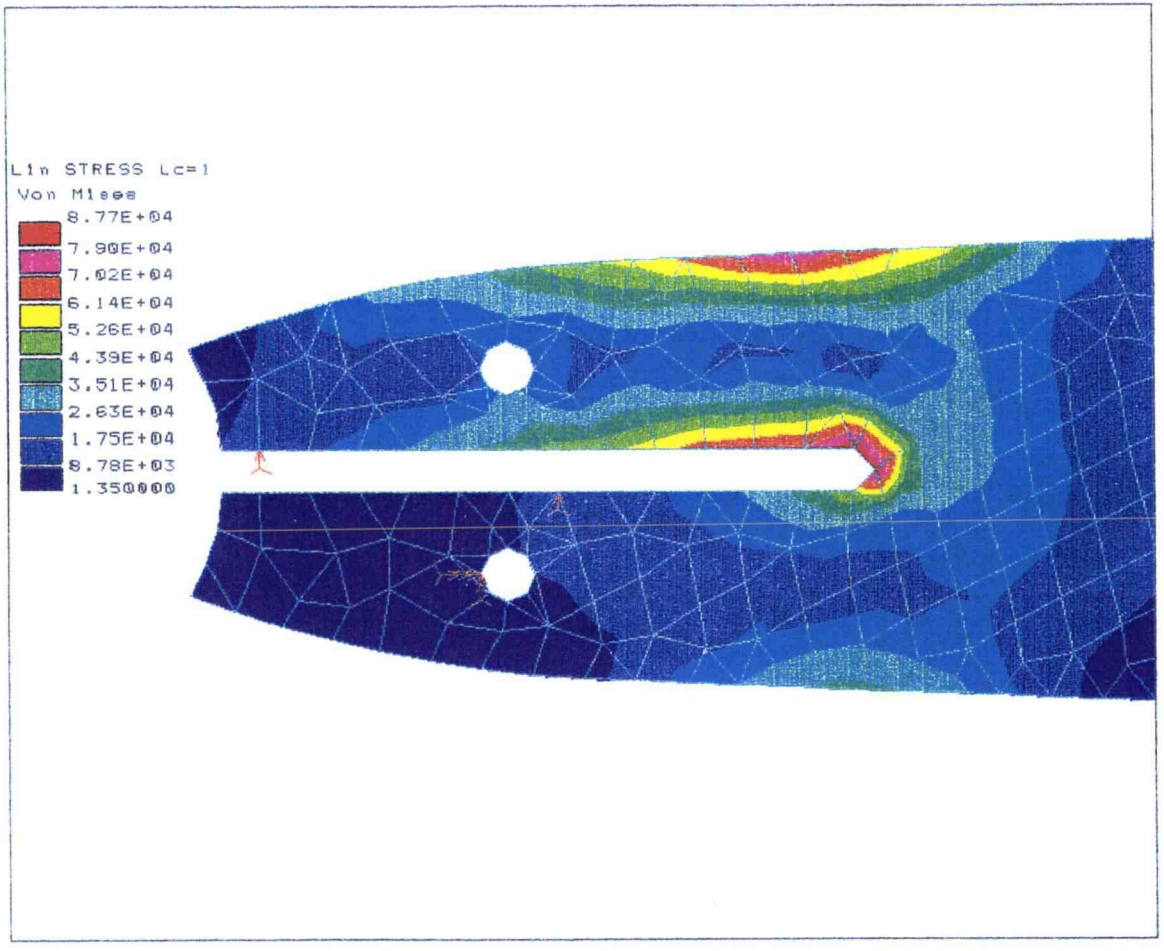

Figure 20. von Mises stress plot for pin supports near back of mounting slot.

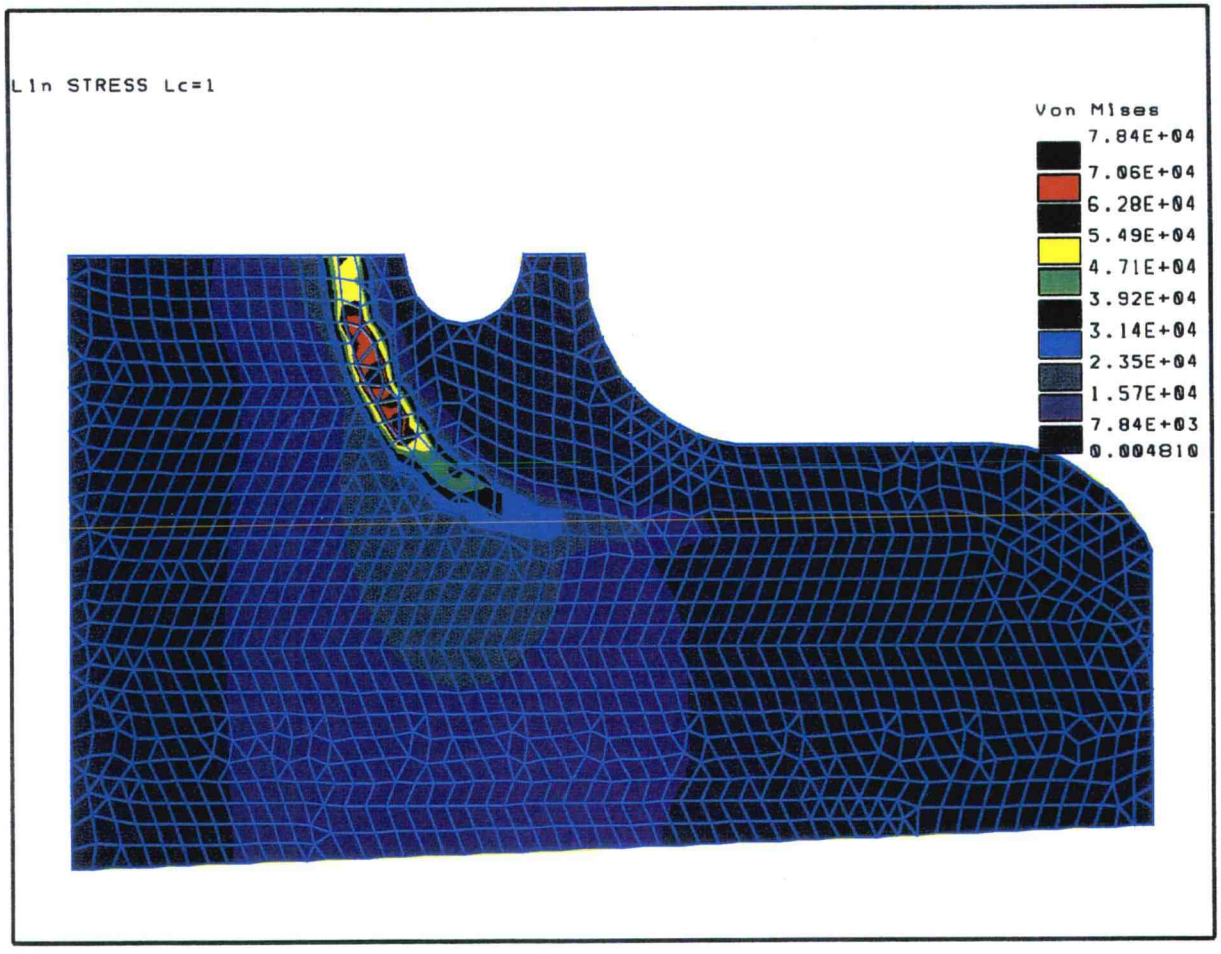

Figure 21. von Mises stress plot of on half of the RSN mounting web.

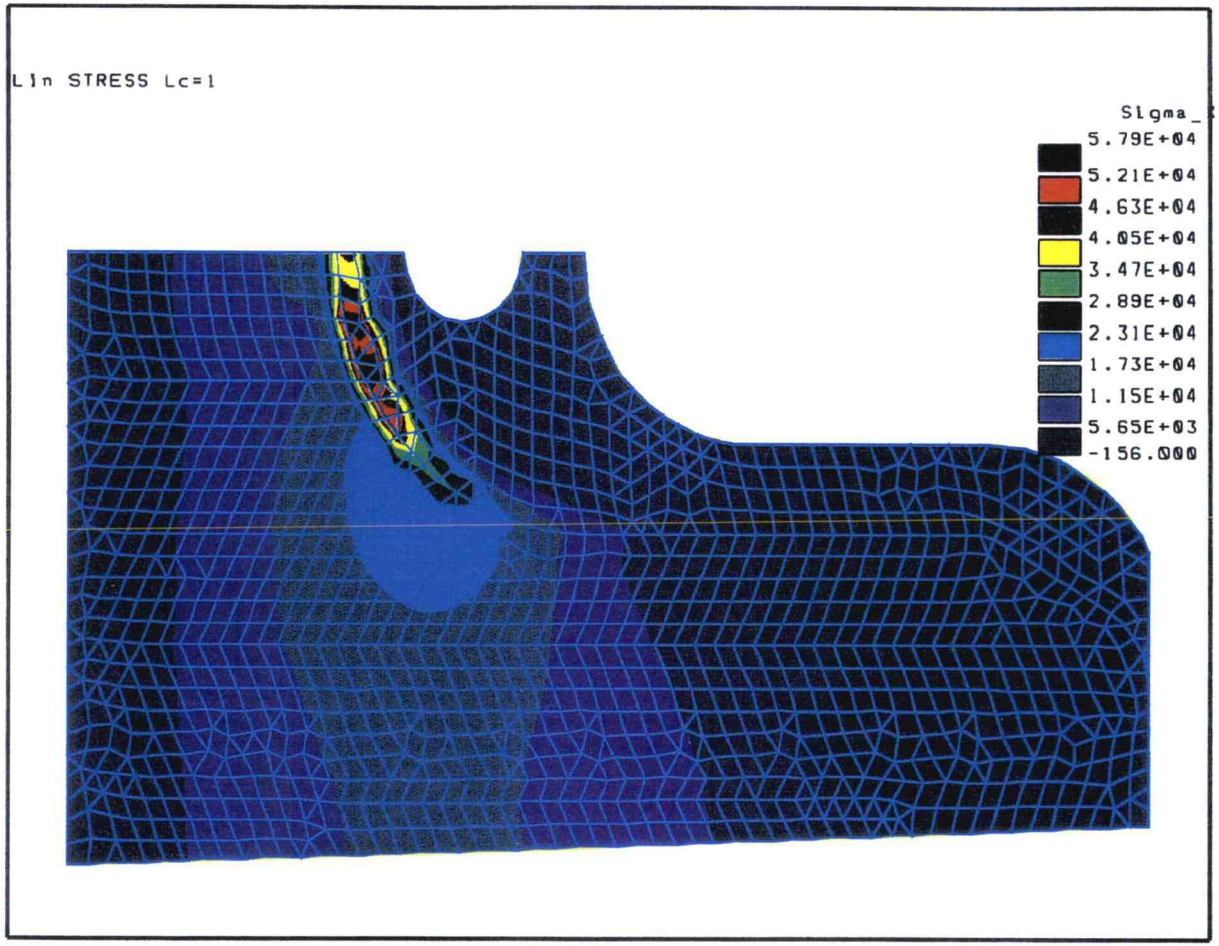

Figure 22. σ_X stress plot of one half of the RSN mounting web.

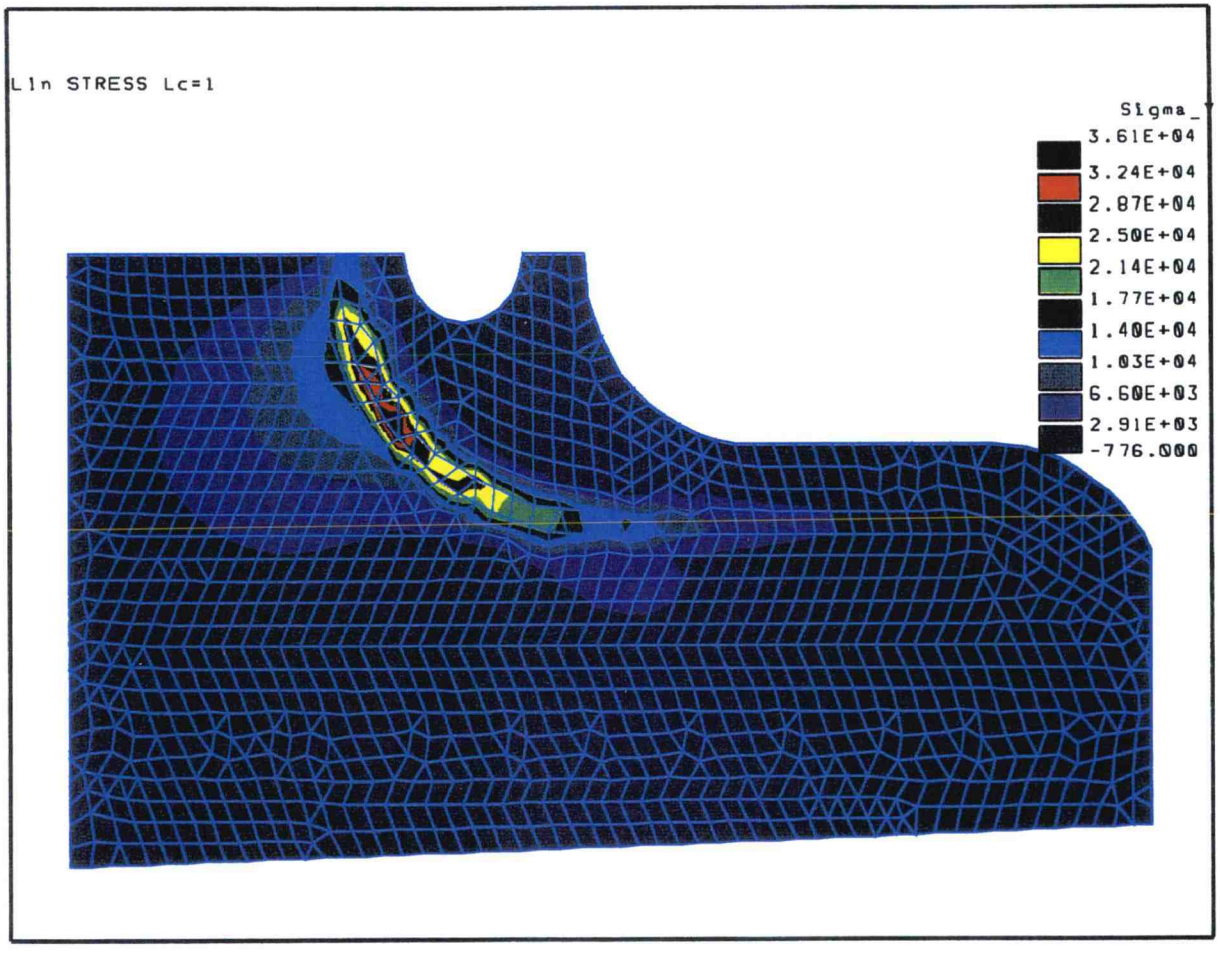

Figure 23. σ_Y stress plot of one half of the RSN mounting web.

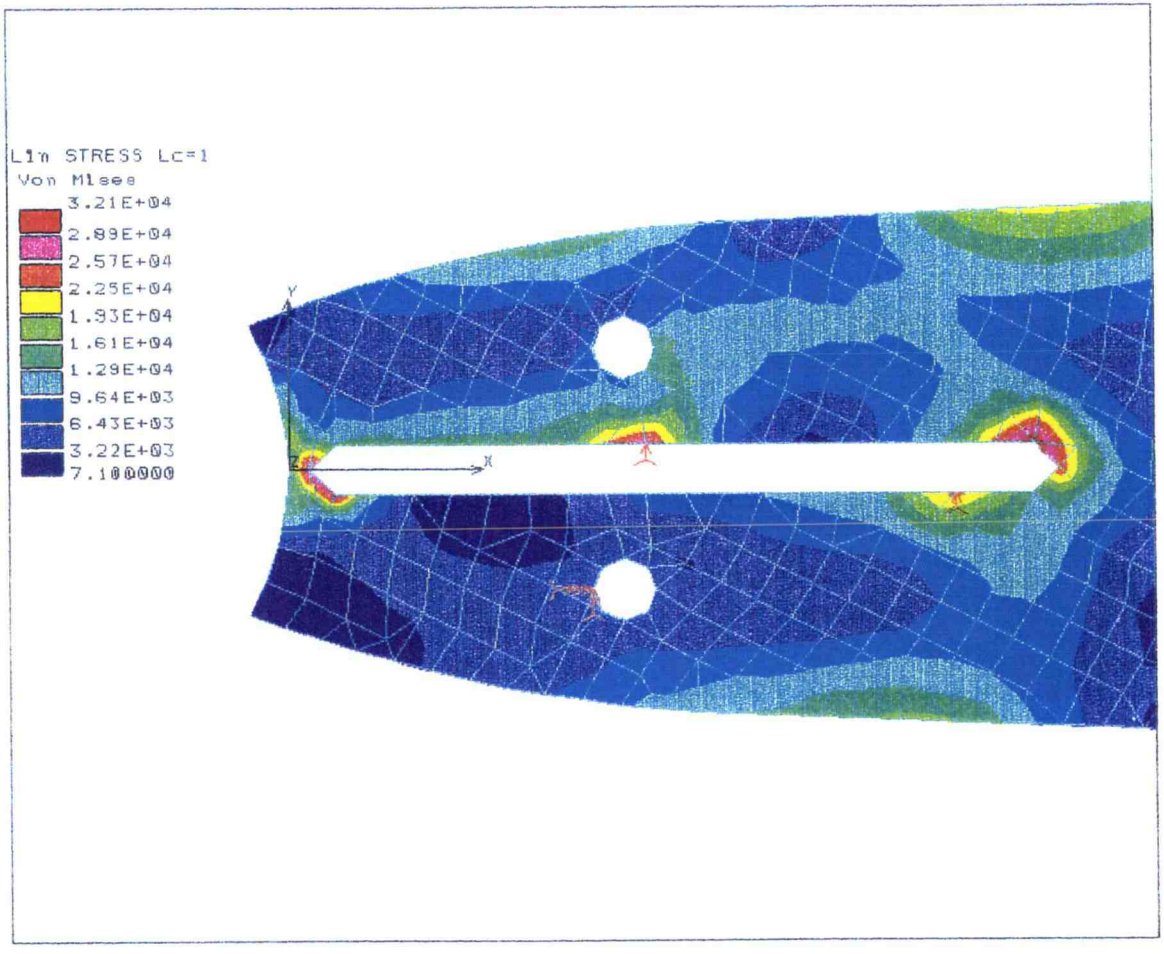

Figure 24. von Mises stress plot for the closed mounting slot with studs near the front.

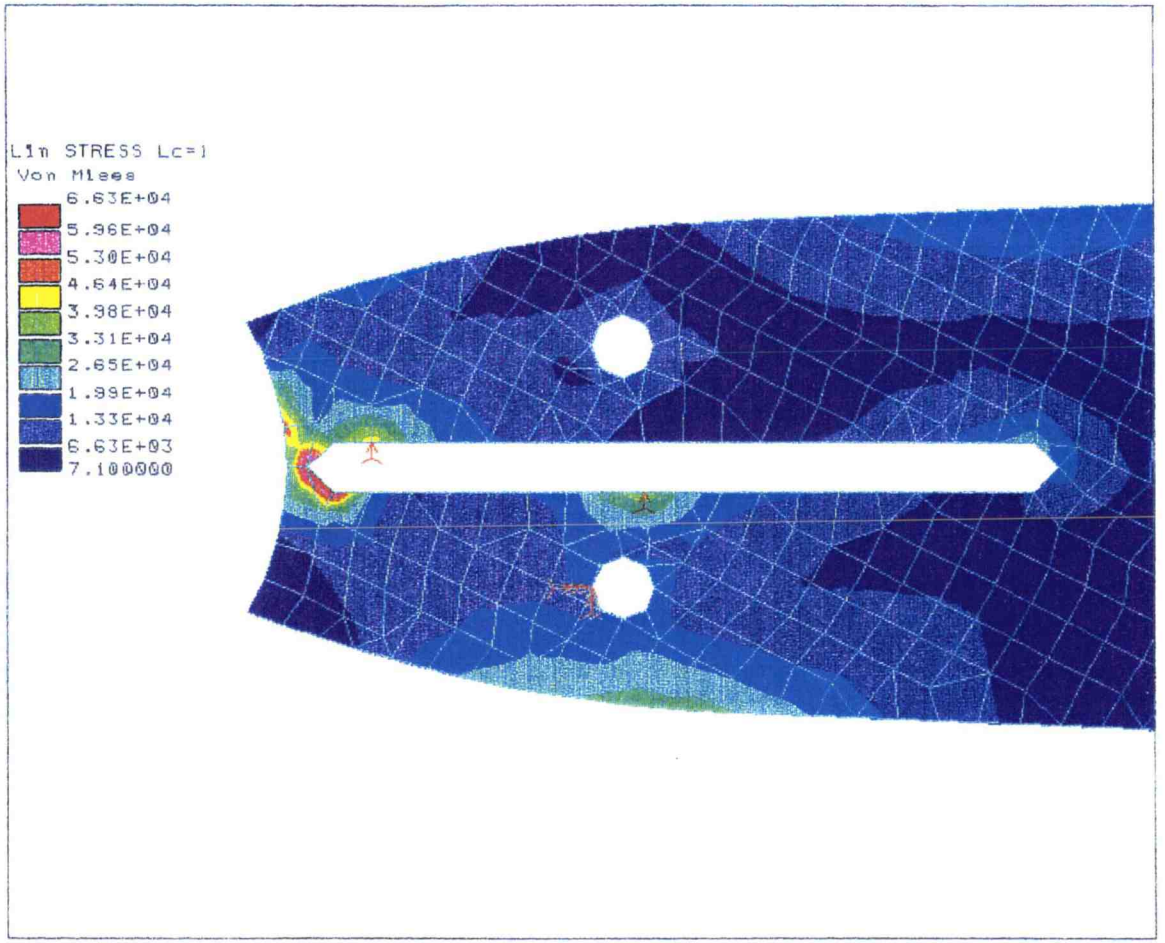

Figure 25. von Mises stress plot for the closed mounting slot with studs near the back.

Beam Theory Verification

Classical beam theory was used to verify the FEA results for the out-of-plane bending configuration. For a guide bar loaded out-of-plane, 35 inches ahead of the mounting region of the bar with 10 lbs, the stress at the outermost fiber is 22,340 psi. For a 20 lb load the stress is doubled resulting in 44,680 psi. For these calculations the bar is assumed to be completely solid including the rails. The base dimension is 0.192 inches and the height of the bar is 2.55 inches at this point.

These calculations compare very well to the FEA model for out-of-plane bending with the same load and configuration (see table 3). Figure 17 gives the peak stress ahead of the mounting region to be 50 ksi. The low value for this same region is approximately 40ksi. The average value of 45 ksi results in only 0.71% difference between to FEA and classical approaches.

Table 3. Comparison of FEA results and classical beam theory calculations.

	FEA results	Classical beam theory	% error
10 lb out of plane test	22500 psi	22340 psi	0.72 %
20 lb out of plane test	45000 psi	44680 psi	0.72 %
50 lb in plane test	8240 psi	8410 psi	2.0 %

Classical beam theory used for in-plane loading of the bar with 50 lb load, 35 inches from the mounting region, shows the maximum stress of 8,410 psi occurs at the outermost fiber. The FEA result from figure 18 was 8,240 psi. This represents a difference of only 2%. After comparing the classical results with the FEA analysis it is evident that the FEA

models represent the actual guide bar behavior. It is also evident that the guide bar behaves very much like a beam in bending in the classical sense.

Strain Gauge Verification

As explained in the procedure section of this paper, strain gauges were used to additionally verify the finite element results. In order to obtain complete strain information in the plane, rosette gauges were used. As shown in figure 8, the gauges were positioned in one of the highest strain areas of the bar; just ahead of the mounting region (compare with figure 18).

The bar was loaded in the out-of-plane configuration as well as in-plane. The bar was loaded with 10 and 20 lb in the out-of-plane tests and 45 lb for the in-plane tests.

Table 4 gives the actual strain readings. Note that all strains are reported as microstrains.

Table 4. Micro-strains for 10 and 20 lb, out-of-plane, tests and 45 lb in-plane test.

Strain gauge	10 lb test	20 lb test	45 lb
$A\varepsilon_0$	711	1388	25
$A\ \varepsilon_{120}$	-14	-31	20
$A\varepsilon_{240}$	95	189	70
$B\ \varepsilon_0$	739	1425	-345
$B\varepsilon_{120}$	41	123	-20
$B\ \varepsilon_{240}$	18	31	115

Table 5 reports the principal strains and the angle to the principal strain axis from the 0° strain gauge. These values were calculated from equations 9 and 10.

Table 5. Principal micro-strains for the out-of-plane and in-plane strain gauge tests.

principal strains and angle	10 lb test out of plane	20 lb test out of plane	45 lb test in plane
A ε1	715	1397	70
A ε2	-187	-367	6
A α	-4°	-4°	33°
B ε1	739	1427	190
B ε2	-207	-374	-356
B α	1°	2°	8°

The principal stresses can be found in tables 6 and 7. For the sake of completeness, the angles to the principal stress/strain axis are repeated from table 5. In addition, appropriate values from the FEA analysis are included in tables 6 and 7 for comparison. The stress values were calculated from equation 11 which relates the stress to the strain via the Youngs modulus (E). Youngs modulus was assumed to be 30×10^6 psi for steel.

Comparing the out-of-plane strain gauge results against the FEA analysis and classical analysis, gives further evidence that the FEA models correctly predict the actual bar behavior. For the out-of-plane loading condition the strain gauge results differ by 7% with the FEA analysis and 6% with the classical calculations.

Table 6. Comparison of FEA and strain gauge results for out of plane tests.

principal stresses and angle	10 lb out of plane		20 lb out of plane		
	FEA	Strain gauge	FEA	Strain gauge	Error
A σ1	22500 psi	21450 psi	45000 psi	41910 psi	6.9%
A σ2		5610 psi		-11010 psi	
A α		-4°		-4.14°	
B σ1	22500 psi	22170 psi	45000 psi	42810 psi	4.9%
B σ2		-6210 psi		-11220 psi	
B α		-.8°		1.7°	

Unfortunately the in-plane results are not as convincing. After compensating for the difference in the load of 45 lbs using the strain gauges and the 50 lbs used in the FEA models and classical approach the difference is still significant. The strain gauge stress in the longitudinal direction is 43% lower than the FEA results. The difference is 44% when compared with the classical approach. These results indicate that the strain gauges are not accurately predicting the stresses in this region of the bar under these loading conditions. The apparent error is not entirely surprising considering the stress gradients shown in figure 18 from the FEA analysis. Due to the large foot print of the strain gauge the assumption of constant strains is violated for the in-plane loading condition. Since the purpose of the strain gauge experiment was to validate the FEA model, which was successful, further strain gauge work was not performed. If more accurate results were required for the region ahead of the power head for the in-plane loading configuration smaller rosette gauges would be recommended. In addition, rosettes with the three individual gauges in a stacked configuration would help to decrease the sample area and provide superior results.

Table 7. Comparison of FEA and strain gauge results for out of plane tests.

principal stresses, angle	45 lb test in plane		
	FEA	Strain gauge	Error
A σ1	4885 psi	2100 psi	43%
A σ2		180 psi	
A α		33°	
B σ1	4885 psi	5700 psi	16%
B σ2		10680 psi	
B α		8°	

Results from Differential Scanning Calorimetry (DSC)

Polymer matrix characterization was performed on both PPS and PEI polymer samples by Differential Scanning Calorimetry (DSC). A Shimadzu Model DSC-50 was used for these tests.

Figure 26 is a plot of the PPS matrix after cooling at a rate less than 8°C/min (14° F/min) from 350°C (662°F). Important data discovered from this test include the glass transition temperature (Tg) and the melting temperature (Tm). These values were 104°C (219°F) and 281°C (538°F) respectively. The Tg represents the upper endurance temperature for the product in service. The melting temperature is important for purposes of processing. At or above Tm the thermoplastic can be expected to flow sufficiently to provide good consolidation. The absence of the heat of crystallization hump between the glass transition and the melt temperature is evidence that this material is crystalline.

Figure 27 is a DSC plot for the same PPS thermoplastic after it had been quenched from 350°C (662°F) in liquid nitrogen. Tg for this plot is 97°C (206°F) and Tm is essentially the same as the value from the previous plot.

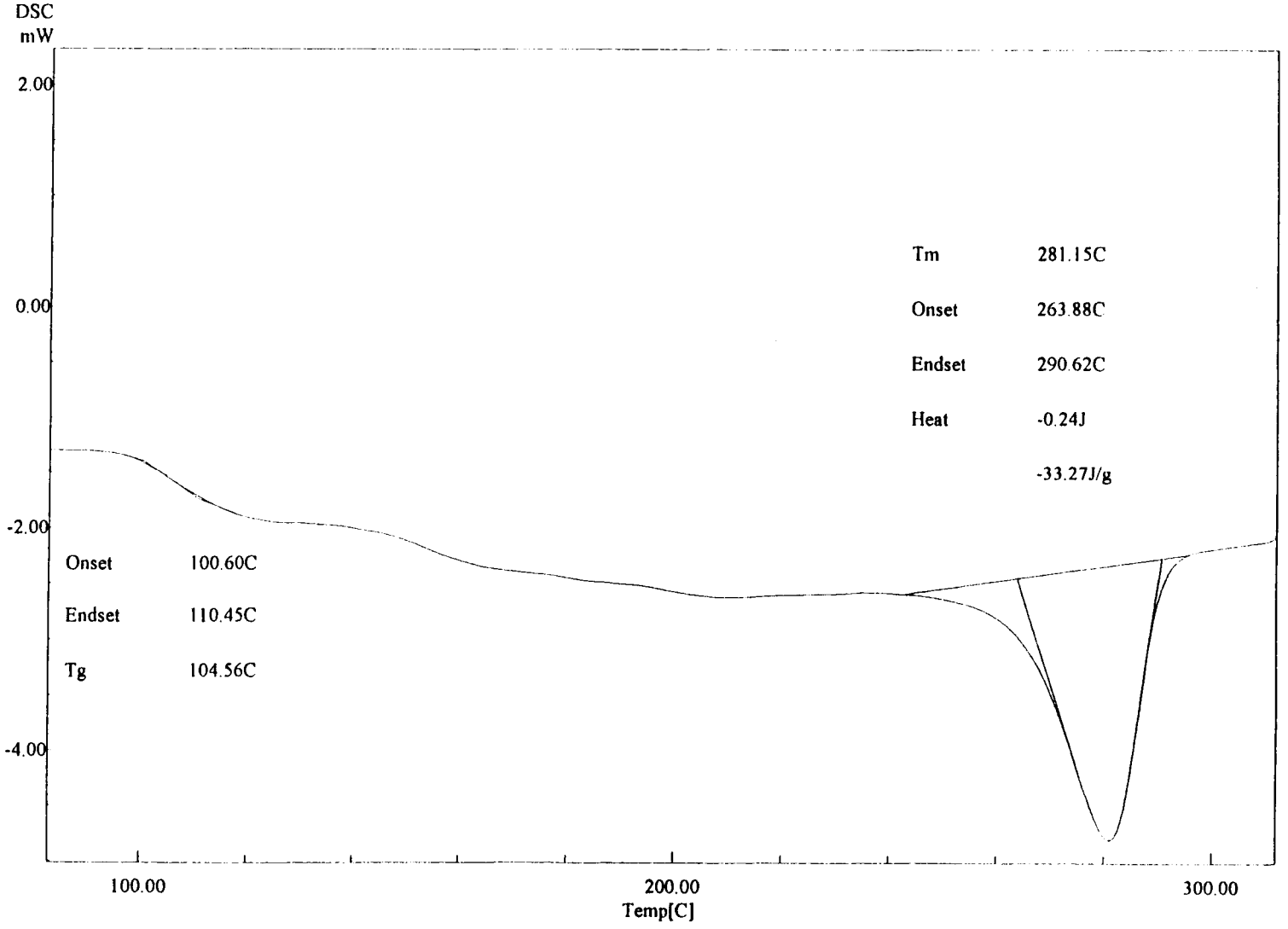

Figure 26. DSC plot of crystalline polyphenylene sulfide (PPS)

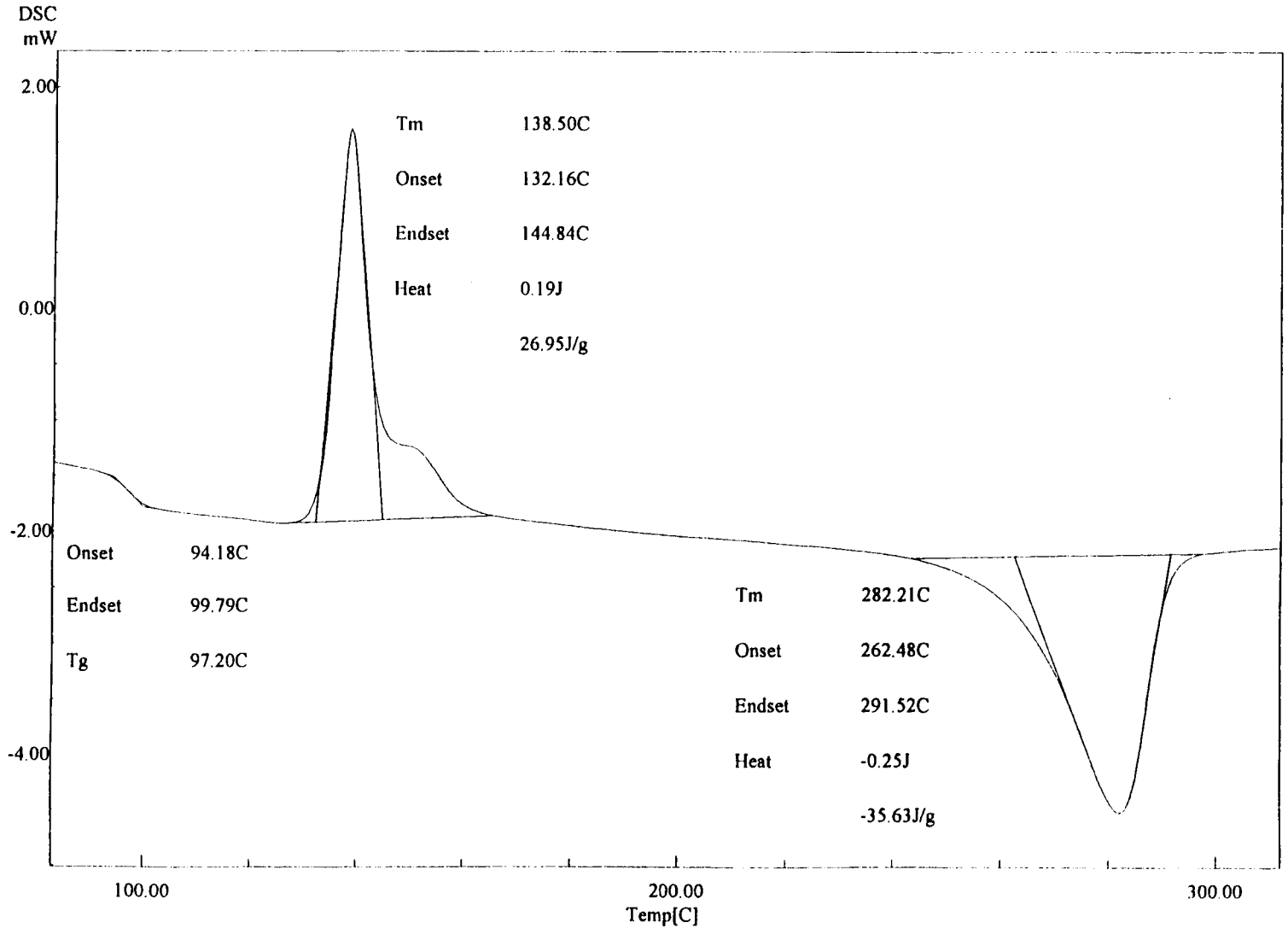

Figure 27. Plot of amorphous polyphenylene sulfide (PPS)

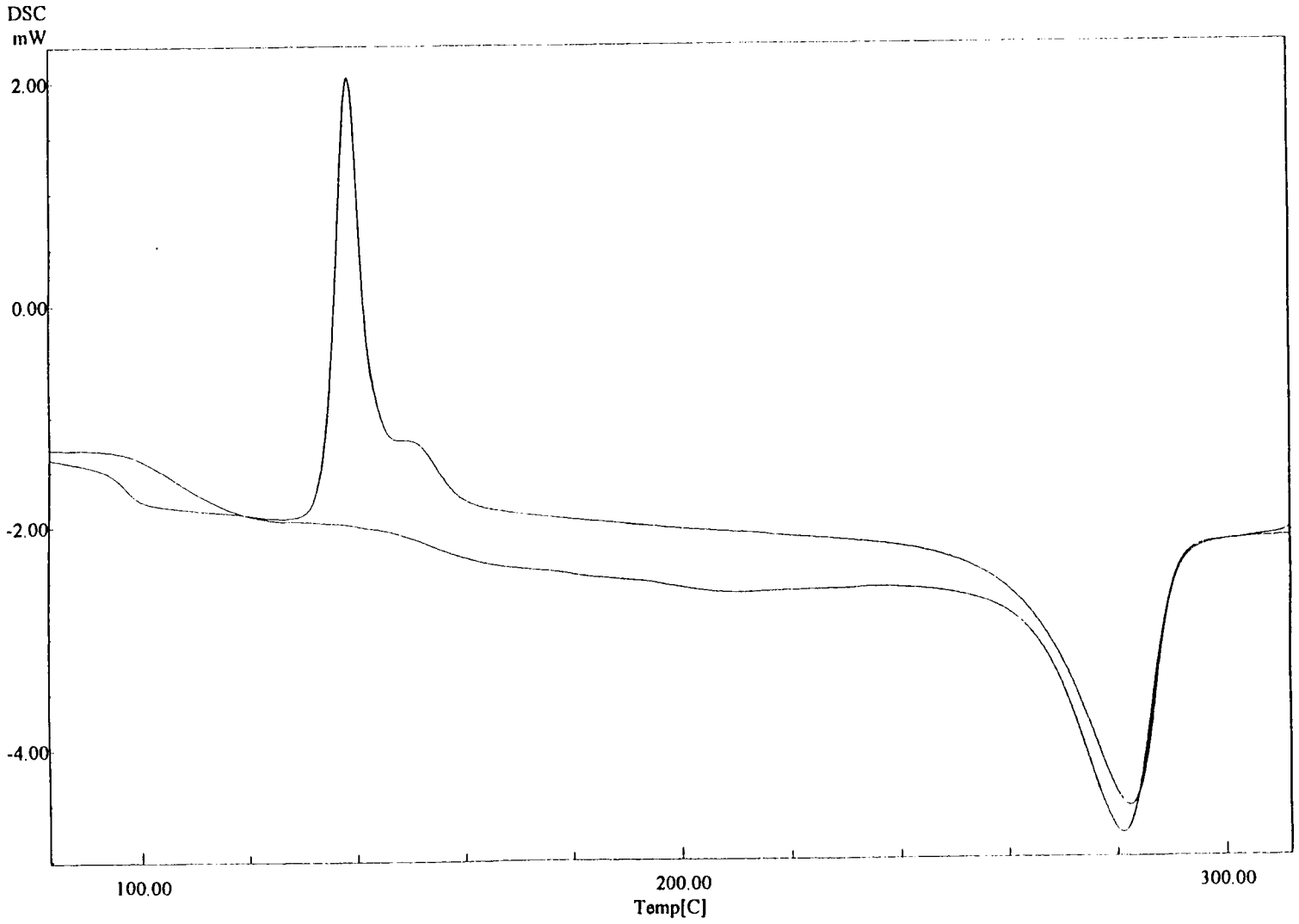

Figure 28. DSC overlay plot of crystalline and amorphous PPS.

The most striking difference between the two PPS plots is the heat of crystallization hump at 138°C (280°F) for the quenched sample. This is the crystallization temperature (Tc), (due to the analysis algorithm this value is reported as Tm on the plots). This indicates that molecular reordering in the PPS sample is occurring, resulting in crystal growth. By rapidly quenching the polymer from the melt, crystallization was inhibited. Once Tc was reached, the molecules had sufficient mobility to reorder into the preferred crystalline structure. The area under this heat of crystallization curve is proportional to the degree of crystallinity for the polymer. At elevated temperatures the material must first pass though the crystallization region before becoming less viscous. This can add some short term dimensional stability at temperatures above Tg for amorphous forms of crystalline polymers including PPS.

For comparison, the amorphous and crystalline PPS curves discussed above, are overlaid in figure 28. It is interesting to note that the slight bump in the curve to the left of the Tg in the crystalline sample coincides with the Tc for the amorphous sample. This indicates that despite the slow cooling some degree of disorder remained in the crystalline sample.

The literature claims that polyetherimide is an amorphous thermoplastic. Figures 29 an 30 indicate that PEI is indeed non-crystalline. Neither plot gives any indication of crystalline peaks as revealed in the PPS plots. The PEI plots show a distinct Tg near 223° C (431°F) and no apparent melt temperature. As the amorphous PEI moves beyond the Tg the viscosity begins to decrease from a tough leathery material to a more fluid material there is no defined melt temperature. The lack of a melt temperature is a characteristic of amorphous polymers. The processing temperature is the temperature at which the plastic flows sufficiently to provide good consolidation.

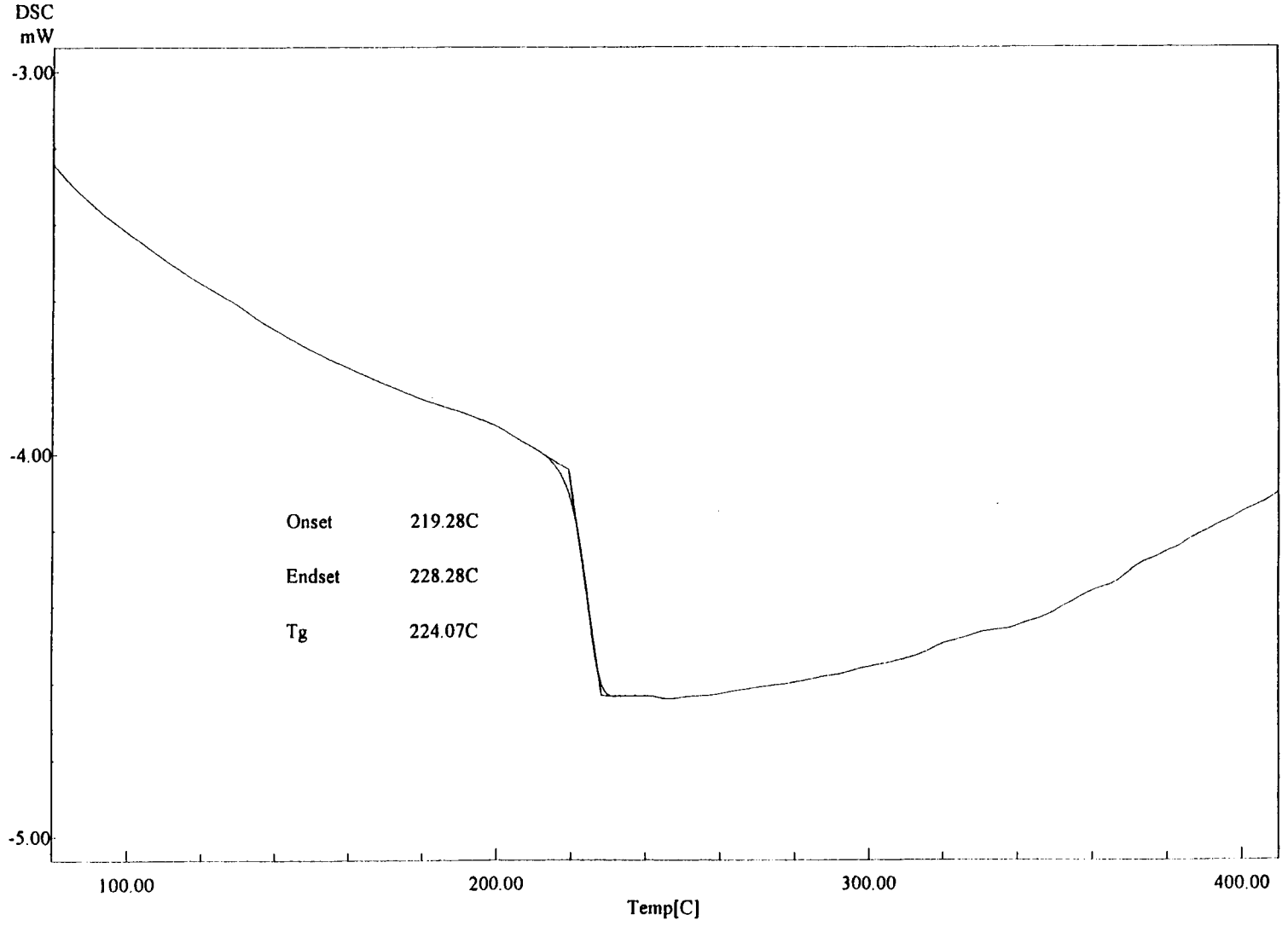

Figure 29. DSC plot of quenched polyetherimide (PEI).

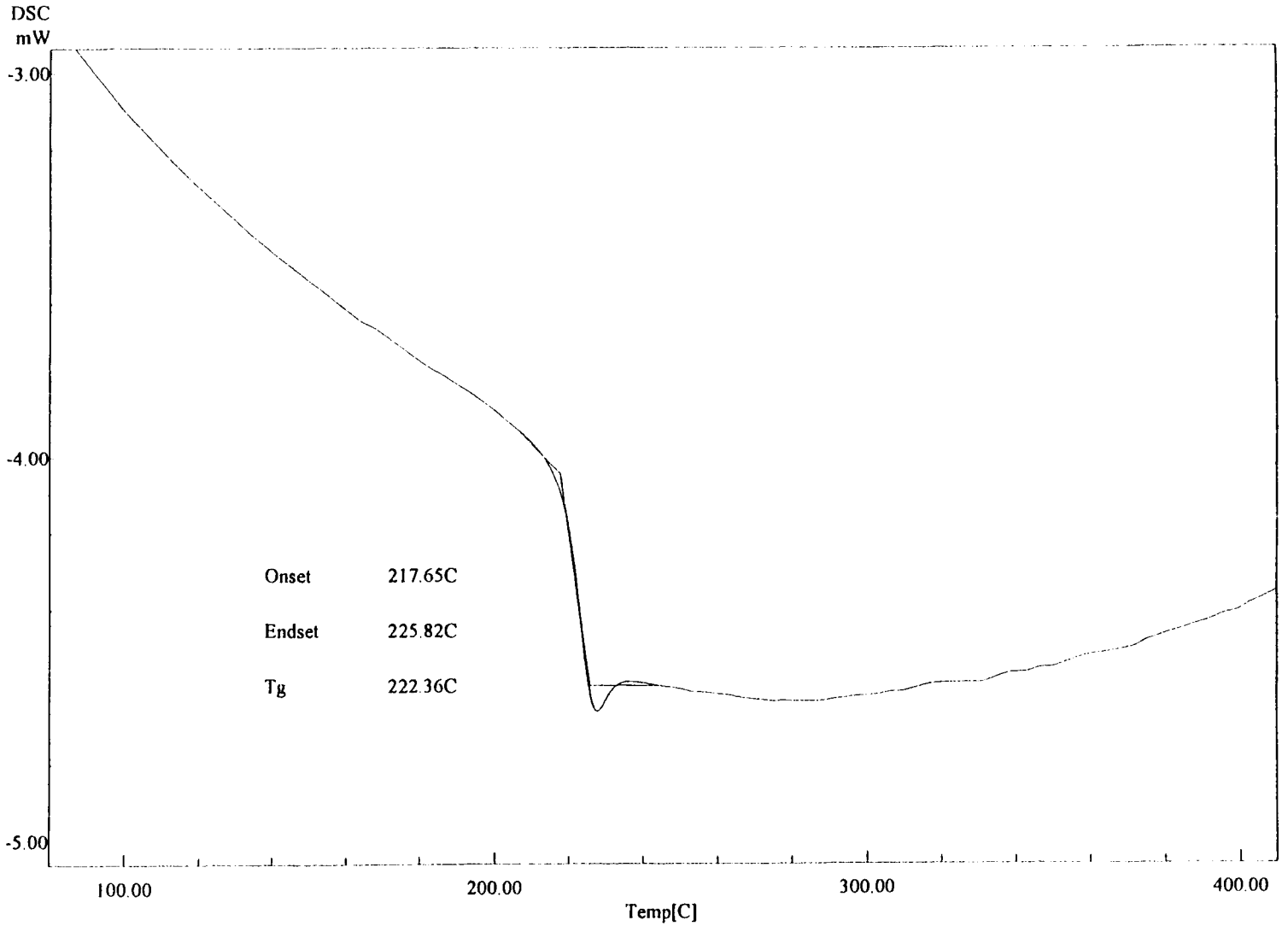

Figure 30. DSC plot of slow cooled polyetherimide (PEI).

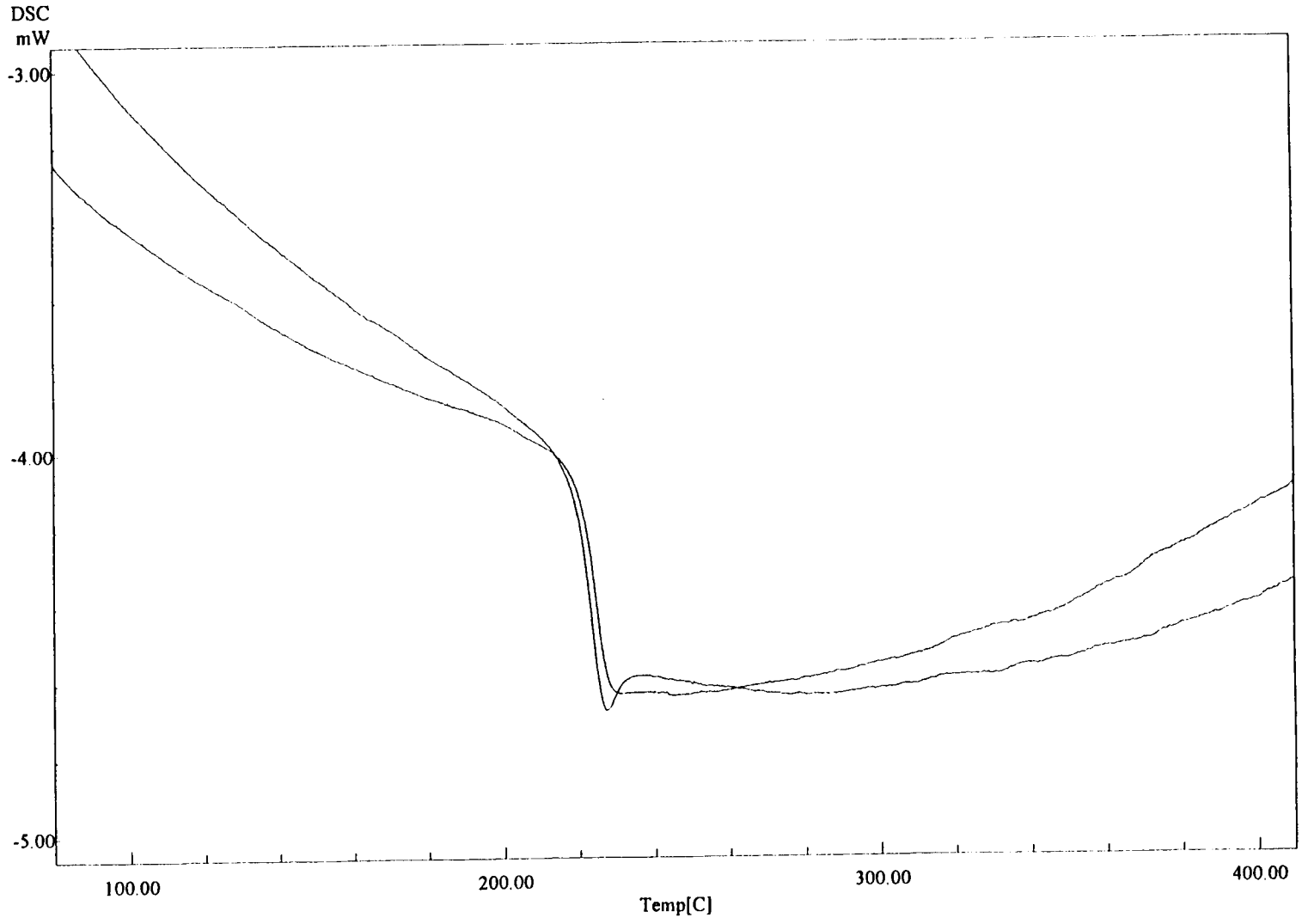

Figure 31. DSC overlay of quenched and slow cooled PEI plots

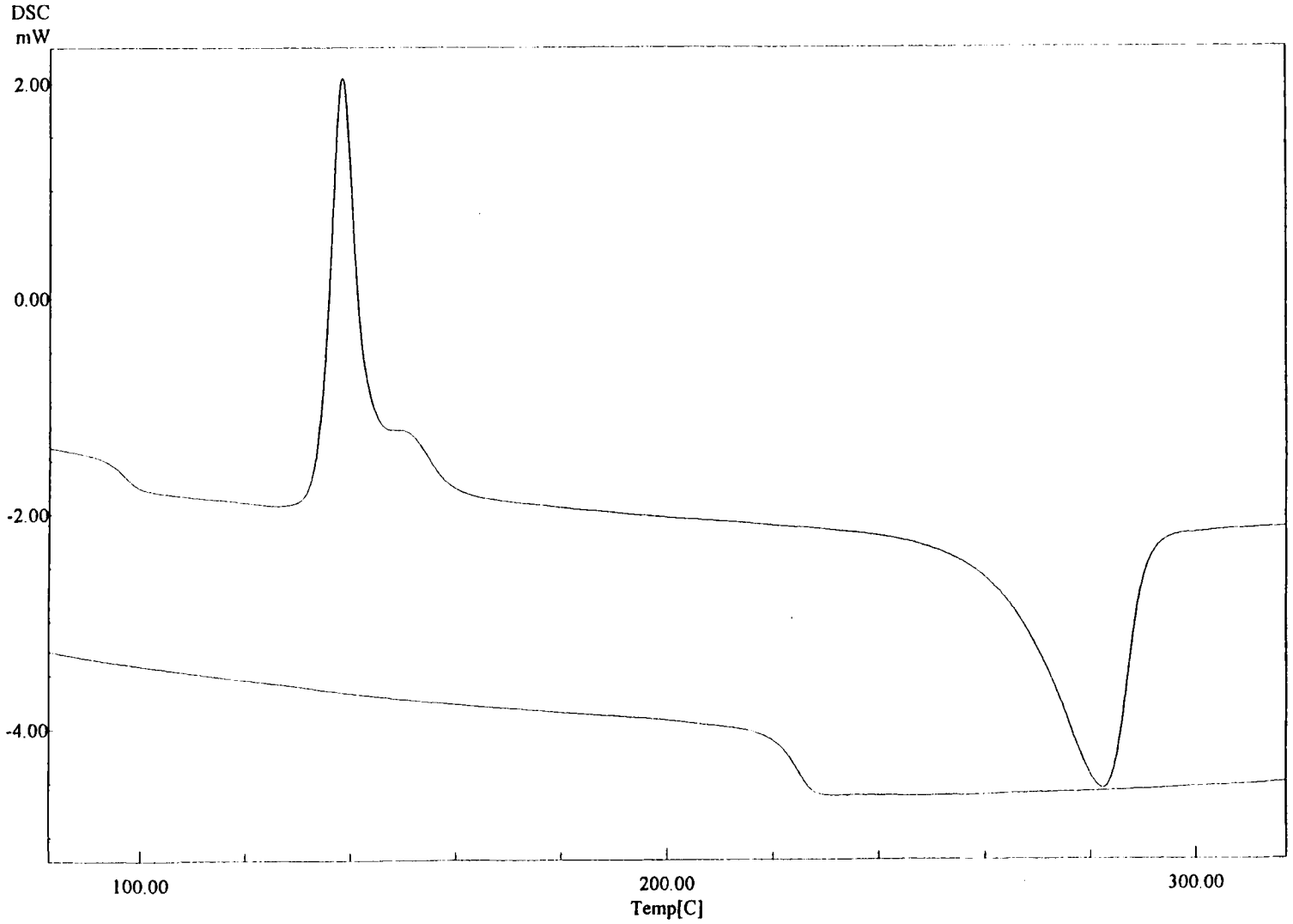

Figure 32. DSC overlay of quenched PPS and PEI plots.

Figure 31 is an overlay of the quenched and slow cooled PEI plots. Both plots exhibit the same general trends and very similar Tg values.

Figure 32 is an overlay of the quenched PPS and PEI plots. The higher Tg for PEI is evident in this plot.

Elastic and Viscous Characteristics

Dynamic mechanical testing was performed to determine the elastic and viscous properties of the PPS and PEI polymer matrices as a function of temperature. A Rheometrics RSA-II solids analyzer was used for these dynamic tests.

Figure 33 is a plot of elastic modulus (G'), loss modulus (G") and the log of the tangent of the phase difference between these moduli as a function of temperature. The rise in G" and tan(δ) towards the left of the chart, can be associated with the Tg of the polymer. The large change in these parameters towards the left is an indication of the melt temperature. Figure 34 plots tan(δ) and data collected from the DSC testing described in the previous section. The dynamic test data for the carbon/PEI lay-up can be found in figure 35.

Figure 36 is a plot of the DSC data and the tan(δ) against temperature. There is no melt temperature evident, which corresponds to an amorphous material.

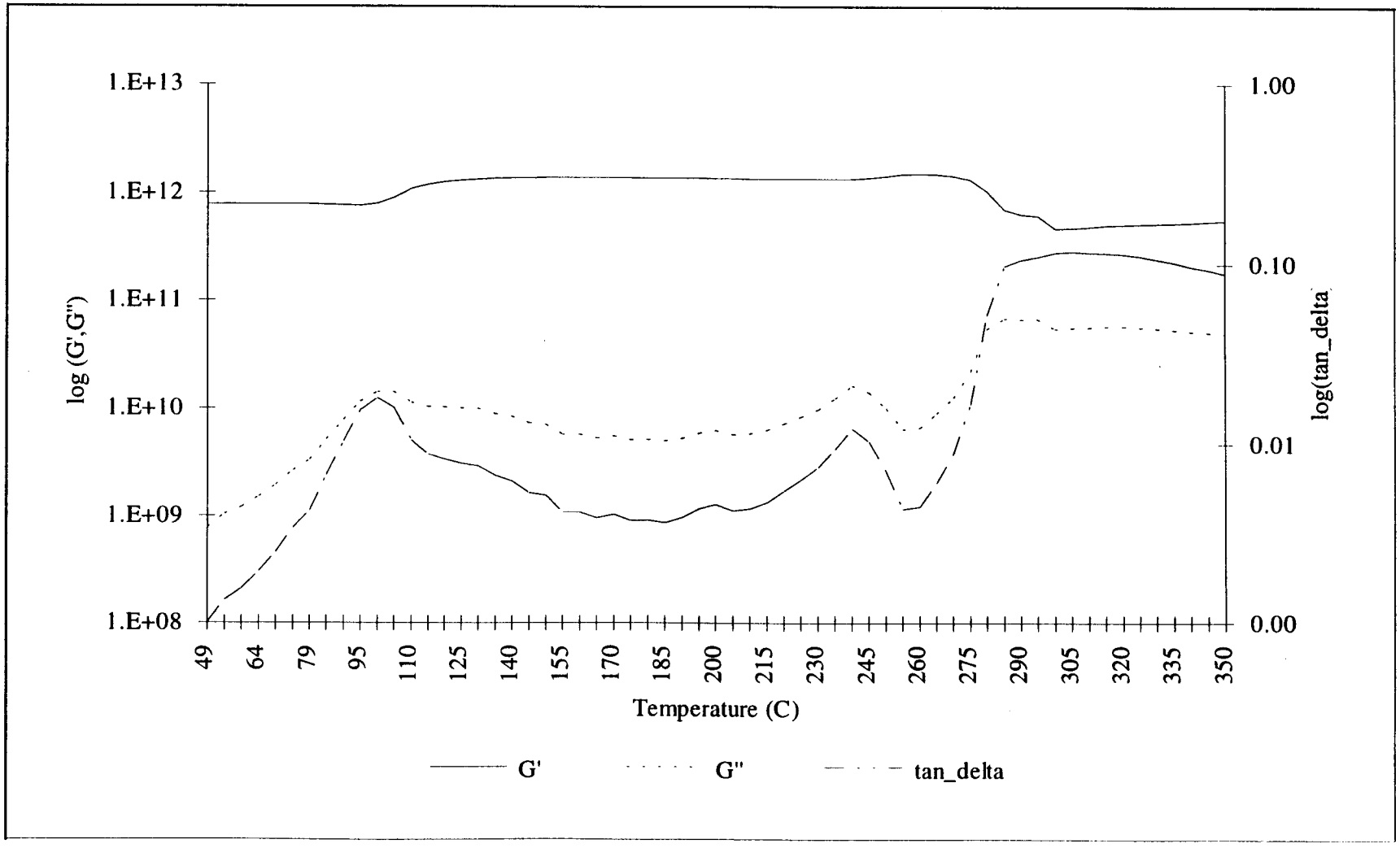

Figure 33. Plot of elastic and loss moduli and tan(δ) for PPS

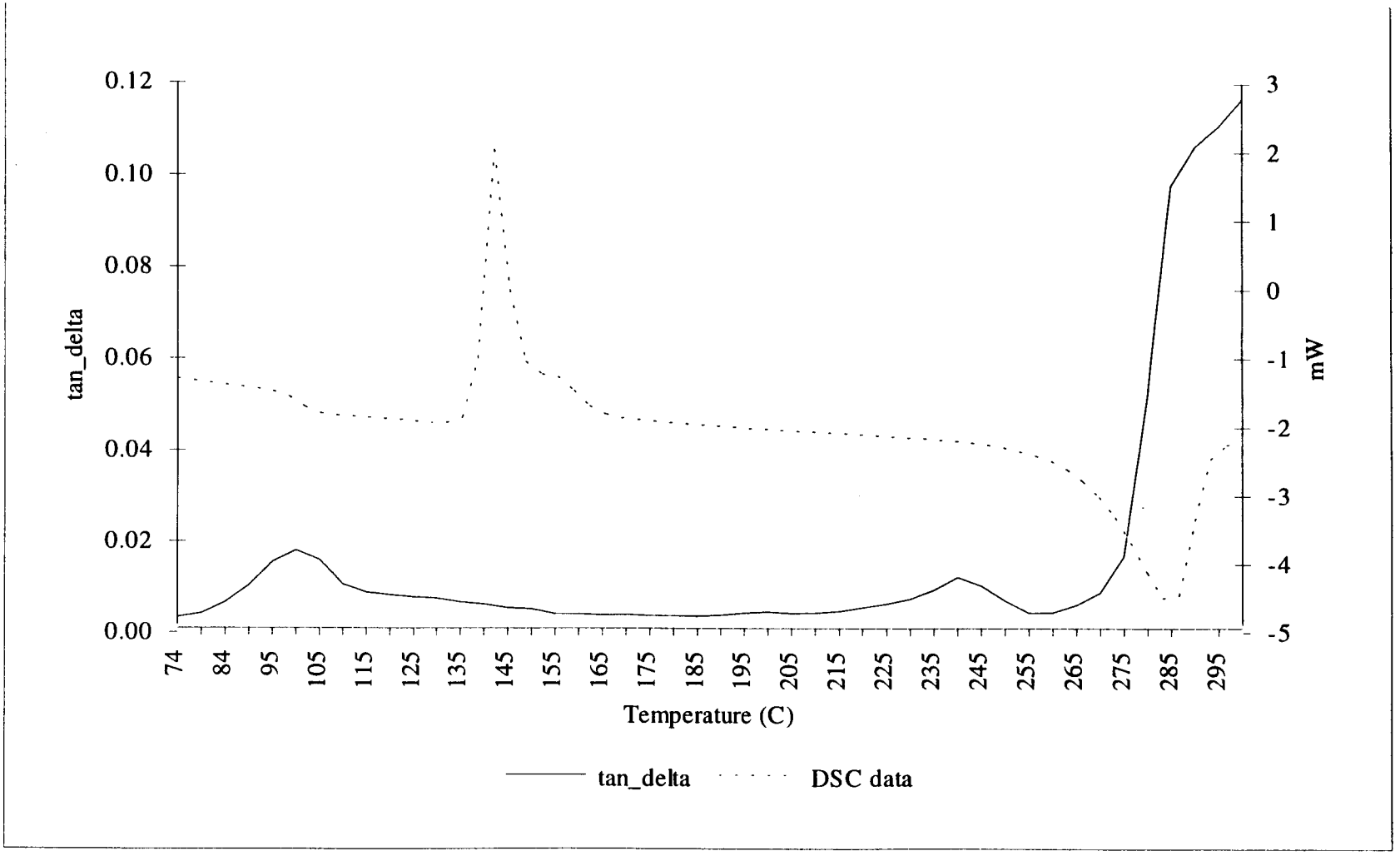

Figure 34. Overlay of tan(δ) and DSC data for PPS.

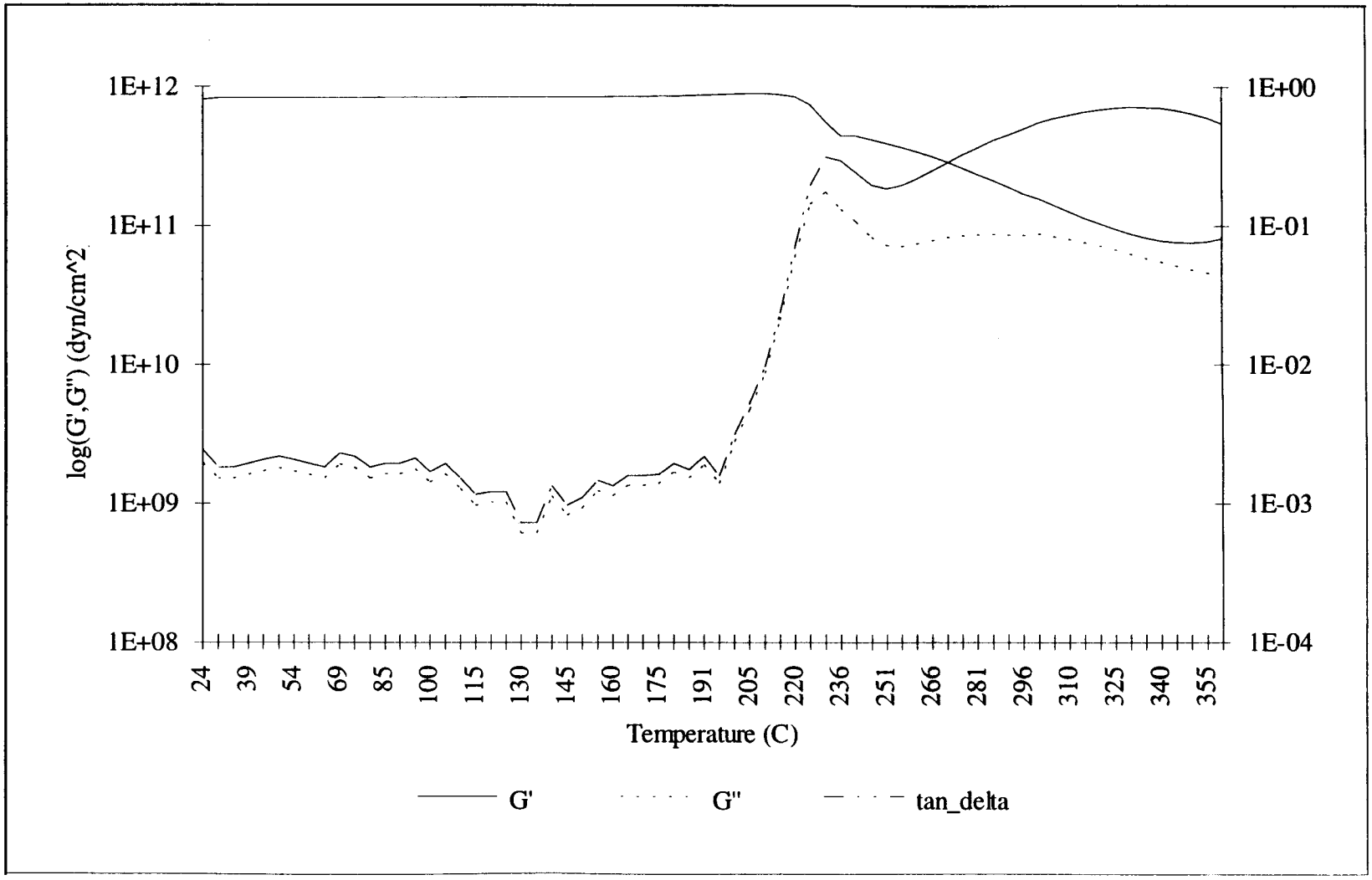

Figure 35. Plot of G', G'' and tan (δ) for PEI.

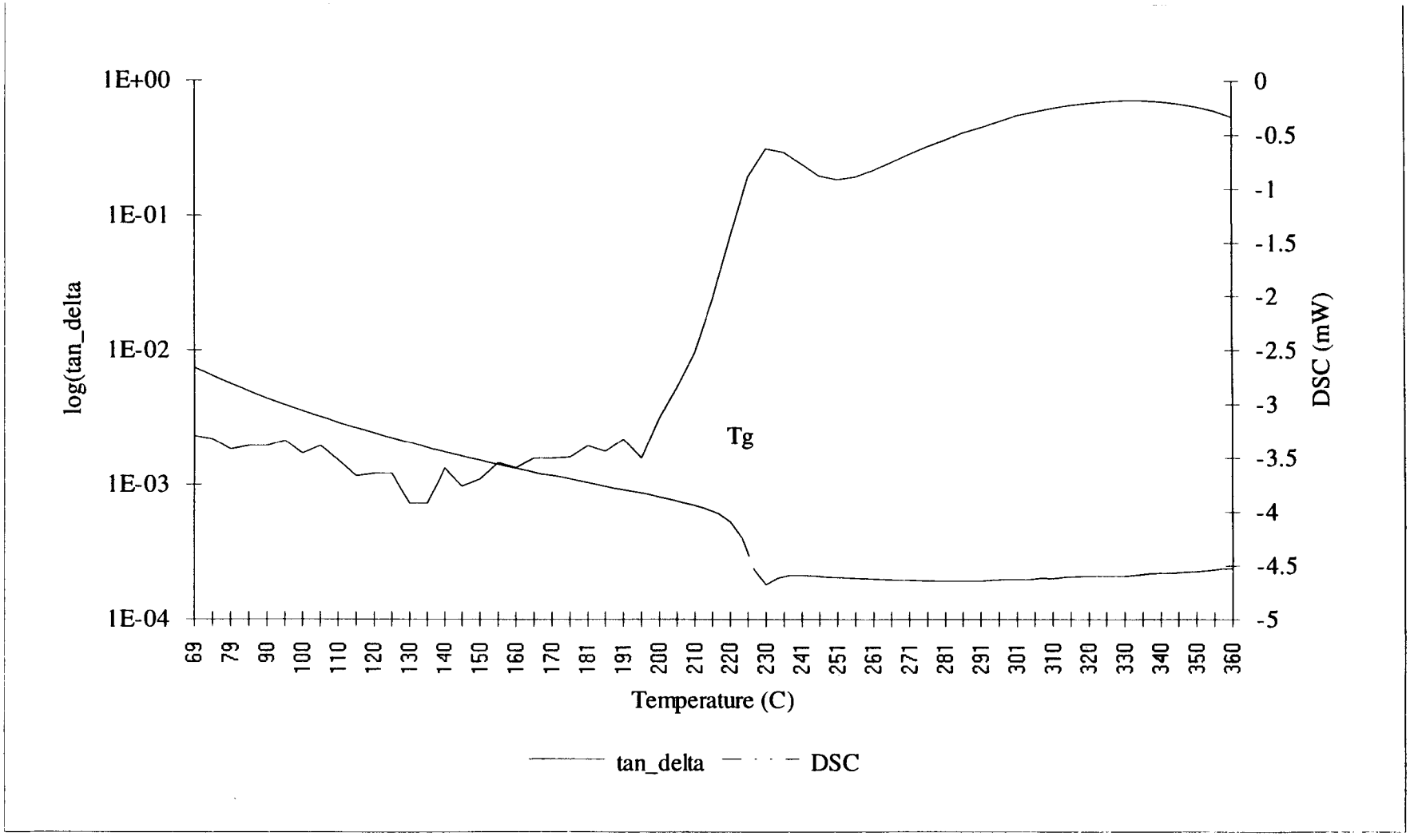

Figure 36. log(tan(δ) and DSC data for PEI.

Non-adhesively Bonded Hybrid Bar

As mentioned in the preceding chapter, the first hybrid bar was fabricated without an adhesive between the composite and steel laminates. Bonding the steel laminates and consolidating the composite was accomplished in one step at 600°F. The thermoplastic matrix acted like the adhesive for the system.

Initially, the non-adhesively bonded hybrid bar appeared to be structurally sound. However, over the course of 2 weeks at room temperature the thermoplastic/steel interface began to slowly fail as one of the steel laminates peeled away from the composite core. Over the next two months 75% of the bond-line at one composite/ steel interface had failed.

This failure is a prime example of the stress developed from differing coefficients of thermal expansion (CTE). In the longitudinal direction carbon fiber has a negative CTE. Unlike most materials, carbon fiber shrinks in the longitudinal direction as it is heated. Steel in contrast has a positive CTE; it expands upon heating.

The bond between the steel and thermoplastic was formed at some elevated temperature; presumably near the Tg since at this temperature the polymer chains are unable to move freely (heat deflection data for this material suggests that this temperature may be as high as 500°F). As the bonded materials cooled to room temperature the carbon fiber composite grew in the longitudinal direction. The steel, being isotropic, shrank in all directions as it cooled. The differential between the two materials developed a sheer stress. Failure of the bond between the composite and steel is evidence that the shear stress developed was greater than the shear strength of the thermoplastic bond.

The non-adhesively bonded hybrid bar was analyzed using GENLAM (complete results can be found in appendix B). From the estimated temperature differential of 400°F the interlaminar shear stress was calculated to be approximately 50 ksi. Assuming this value is correct, there is little mystery why the bond line failed.

Adhesive Testing

Due to the failure of the non-adhesively bonded bar concept, choosing an appropriate adhesive systems became very important. Manufacturer data for the adhesives did not typically include values for thermoplastic composites. For this reason it was necessary to perform adhesive testing.

Table 8 contains the results of the cleavage testing. The Ciba Geigy product Araldite2042 was notable for its good toughness. This product maintained good cleavage strength even after the bond had begun to fail. Unfortunately, the stiffness of the material was very low, much like a hard rubber. This precluded its use in the hybrid guide bar due to the need for a stiff bond between the laminates and a stiff final product.

Table 8. Performance rankings for adhesive cleavage tests.

Product	Toughness	Shear Stiffness
2042	1	6
DP805	2	2
DP460	3	3
DP 420	3	3
2043	5	5
2214 high temp	6	1

The 3M product 2214 high temp was a metal filled one part epoxy. Unfortunately, this product was on the lower end of the testing scale due to extremely poor cleavage strength. This material has extremely good shear stiffness and is reported to have

exceptional high temperature properties. However, once cleavage of the bond surface had initiated the entire bond line failed very rapidly. The laminates literally popped apart.

The final choice for the hybrid bar adhesive was 3M's DP805. This product is a two part acrylic adhesive which bonds well to a variety of surfaces including slightly dirty or oily surfaces. The shear stiffness was determined to be acceptable and the cleavage strength was very good. Once cleavage had begun, the adhesive tended to adhere to the surfaces unevenly. As cleavage progressed the adhesive was forced to tear where it had adhered to opposite layers. This characteristic improved the overall cleavage strength and resistance to debond dramatically. In contrast, most of the other adhesives adhered better to either the top or the bottom substrate. Once failure had initiated it progressed rapidly with little additional force.

Bar Testing

The adhesively bonded hybrid bar was tested on a Husqvarna Model 281XP power head. The bar was attached to the power head with a loop of chain corresponding to the 36 inch bar length and tensioned. Initially the chain could not be easily moved around the bar when moved by hand. This is believed to be caused by small protrusions of adhesive into the chain drive link path. After a few cycles of the chain these impediments had worn sufficiently to allow the chain to move freely around the bar.

The chain saw was started and accelerated slowly. As confidence in the saw and hybrid bar was gained the engine speed was increased without problems. The bar was then used to cut oak logs of various sizes from 4 inches to 28 inches. The bar and power head combination performed extremely well.

After several minutes of cutting a large log fell on the nose of the hybrid bar. This sudden shock caused 0.3 inches of the adhesive bondline between the nose web and the

steel side laminates to fail. This allowed the chain to jump off the bar. The bar was then repaired with a small amount of DP805 and the bar was returned to service.

The all composite bar was briefly tested by Oregon Cutting Systems (OCS) Division of Blount, Inc. Apparently the distance between the rails was too tight. This caused excess friction on the drive link of the saw chain. OCS found that the chain became extremely hot to the touch, but the saw bar did not become significantly warmer. It is known that carbon fibers have exceptional high thermal conductivity, especially in the fiber direction. The heat generated by the friction was probably conducted by the carbon fibers away from the rails, into the bar body and then radiated to the air by convection.

OCS found that the bar rails tended to wear faster than the equivalent steel bar. This tendency was most pronounced near the drive sprocket mounting region of the bar.

CONCLUSIONS

The purpose of this research was to design and fabricate a chain saw guide bar with composite materials. The goal was to design a guide bar with significantly lower density than the current steel construction. The negative impact of the material change on guide bar rail wear and overall stiffness was to be minimized as much as possible. Important factors such as raw material storage and processing requirements were also considered important in material selection. Cost was not stipulated to be a significant factor for this research.

From the general requirements outlined above, carbon fiber reinforced plastics (CFRP) were thought to be the best choice. Carbon fibers offer low density while maintaining "steel like" stiffness. In addition, carbon fiber reinforced materials are readily available. The use of these materials continues to increase in all industries where specific stiffness and strength are important.

Thermosetting polymers, such as epoxies and vinyl esters, were considered candidate matrix materials with the carbon fiber. However, due to refrigeration requirements and environmental concerns, thermoplastics became the matrix material of choice. In addition, thermoplastics offer generally higher toughness than thermosets and reformability.

From the literature survey, polyphenylene sulfide (PPS) and polyetherimide (PEI) were chosen for further evaluation. These materials had the necessary chemical resistance and elevated temperature properties.

Differential scanning calorimetry (DSC) and dynamic mechanical testing were used to evaluate processing and end use temperatures. From these tests the preferred temperature for consolidation was 600°F. The glass transition temperatures (Tg) for PPS and PEI are approximately 220°F and 430°F respectively. The dynamic mechanical testing, particularly the tan(δ) results, suggest that the upper use temperature for PPS is

approximately 260°C (500°F). From this testing the upper use temperature for PEI was determined to be approximately 205°C (400°F).

Qualitative studies of various structural adhesives were performed to determine relative cleavage properties and stiffness. DP805, a 3M product, was determined to have the best cleavage resistance while maintaining good shear stiffness qualities.

Various heaters, dies and hydraulic press attachments were successfully fabricated. This equipment was used to produce the sample coupons for adhesive and lay-up verification. In addition, considerably larger heaters were fabricated to produce the heaters used for the prototype chain saw guide bars.

Three chain saw guide bars were produced. The first two prototype guide bars utilized a hybrid composite/steel laminate construction. They both had two outer steel laminates bonded to a central core of carbon fiber and PPS. One bar made use of the thermoplastic matrix to bond the composite and steel laminates while the other bar used DP805 acrylic adhesive. The steel side laminates supplied good stiffness and wear resistance. The carbon core added to the overall stiffness of the hybrid design while decreasing the density. This design decreased the weight by 18% from the standard steel guide bar.

The non-adhesively bonded bar was not performance tested due to premature failure of the composite and steel bond line. This failure was caused by the interlaminar shear stress developed during cooling from 600°F to room temperature.

The small adhesive fracture at the nose of the adhesively bonded hybrid bar discussed in the previous chapter illustrates the problems with adhesively bonded joints. This problem can be attributed to the design constraint of using the replaceable sprocket nose assembly. Elimination of this adhesively bonded joint by redesigning the sprocket nose attachment would eliminate this damage point.

The final prototype bar was built entirely of a carbon fiber/PEI laminate. This all composite bar weighed approximately 14 oz. compared to 78 oz. for the steel bar. This results in a 82% weight decrease over the steel bar. The all carbon bar is about 2/3 as stiff as the steel bar and rail wear was found to be higher. The good thermal conductive properties of carbon composites were evidenced in this bar during actual cutting tests.

RECOMMENDATIONS FOR FURTHER RESEARCH

Although this research has been successful, in that two working prototypes were produced, there are always unanswered questions that deserve further study. This brief chapter will outline some of the more important items.

The choice of material used in either the hybrid or the all composite bar still has potential for improvements. For example, LNP Engineering Plastics has a full line of internally lubricated thermoplastic composite materials with fiber reinforcement. One of the categories included in this line of thermoplastics is carbon reinforced Polyphenylene Sulfide (PPS). They also have a line of reinforced Polyetherimide (PEI). Both thermoplastic materials were used extensively in this research project. Various internal lubricants including Polytetrafluoroethylene (PTFE) or Teflon and silicone are used with these thermoplastics. These materials boast significantly reduced coefficients of static and dynamic friction as well as lower wear rates as compared to unlubricated reinforced thermoplastic materials. These materials should be very effective in the relatively poorly lubricated chain saw guide bar system. Use of these materials may offer design flexibility in other areas of the chain saw system as well.

It is recommended that optimization of the fiber orientation for the all composite bar be undertaken. This optimization must be a function of both wear and load. The use of the internally lubricated materials mentioned previously may allow more fibers to be oriented longitudinally without sacrificing low wear rate. Orienting more fibers in this direction will improve the longitudinal stiffness and strength of the guide bar.

Further research for the hybrid composite/steel guide bar should center around utilizing less expensive reinforced composite materials and lowering production cost. For example, it may be possible to use random fiber reinforced thermoplastics rather than the oriented fiber material used in this research. If this type of material was used, plastic

injection mold techniques could be implemented at significant cost reduction for high volume production.

A suggested area of research involves the replaceable sprocket nose (RSN). It is conceivable that this disposable guide bar component could be made more cheaply utilizing random carbon fiber and thermoplastic injection mold techniques. The RSN body could be produced as a single unit rather than the three layer laminate construction currently in use. This would reduce the part count and the labor necessary to assemble and spot weld the steel laminates. It is suggested that the nose sprocket assembly, including the gear like sprocket, bearings and race, currently in production would be used in the composite RSN body.

As discussed in the chapter on procedures DP805 was the adhesive used in the hybrid composite bar. In the two months since the hybrid bars fabrication, a new product with longer pot life was introduced. DP820 is an acrylic adhesive similar to DP805, but with a 20 minute cure time. This product would have been a significant advantage had it existed at the time the hybrid bar was fabricated. This illustrates the point that the composites and adhesives industries are constantly changing as technology improves. New products will continue to be introduced with improved characteristics and lower cost. It is recommended that every effort be made to stay abreast of these improvements.

BIBLIOGRAPHY

1. IAIN THOMSON, Blount, Inc., Private Communication, March 15, 1996

2. NORMAN E. DOWLING, Mechanical Behavior of Materials, Prentice Hall, Englewood Cliffs, NJ, 1993, pp. 51, 89-90, 127.

3. HERCULES, Product Data Sheet, "Hercules® Carbon Pre-preg Tape AS4/1919", September 19, 1994.

4. DON G. BRADY, "Polyphenylene Sulfides (PPS)", Handbook of Composites, Guide to Engineering Plastics Families: Thermoplastic Resins, A. KELLY and S. T. MILEIKA, Editors, pp 188.

5. R.E FINDES and J. P. Bartolomucci, "Polyetherimides Offer Strength and Stiffness", Advanced Materials and Processes, January 1996.

6. ROBERT M. JONES, Mechanics of Composite Materials, Hemisphere Publishing Corporation, NY, 1975, pp. 23.

7. MARTIN VAN DRUEMEL, Ten Cate, Inc., Private Communication, December 11, 1995

APPENDICIES

APPENDIX A: GENLAM Calculations for the Composite Bar Layup

Results from GENLAM calculations for the solid composite bar layup of

[0,0,+45,-45,90,90,90,-45,+45,0,0,0,0,0,0,0,0,0]s

with a moment of 700 in*lb and a temperature differential of -300°F.

Think Composites's GENLAM V

Laminate stiffness matrix

.3059E+07	.1220E+06	-.9198E-02	-.1797E-01	.9087E-03	-.1757E-03
.1220E+06	.1177E+07	-.2092E-01	.9087E-03	.1571E-01	.6841E-04
-.9198E-02	-.2092E-01	.7634E+06	-.1757E-03	.6841E-04	-.2539E-03

-.1797E-01	.9087E-03	-.1757E-03	.9533E+04	.6594E+03	.2117E+02
.9087E-03	.1571E-01	.6841E-04	.6594E+03	.6563E+04	.2117E+02
-.1757E-03	.6841E-04	-.2539E-03	.2117E+02	.2117E+02	.3153E+04

A* B*
3B* D* [msi]

14.160	.565	.000	.000	.000	.000
.565	5.447	.000	.000	.000	.000
.000	.000	3.534	.000	.000	.000

.000	.000	.000	11.351	.785	.025
.000	.000	.000	.785	7.815	.025
.000	.000	.000	.025	.025	3.754

Laminate compliance matrix

.3283E-06	-.3404E-07	.3023E-14	.6240E-12	-.2669E-13	.1503E-13
-.3404E-07	.8534E-06	.2297E-13	-.4523E-14	-.2038E-11	-.6699E-14
.3023E-14	.2297E-13	.1310E-05	.2506E-13	-.1651E-13	.1054E-12

.6240E-12	-.4523E-14	.2506E-13	.1056E-03	-.1061E-04	-.6381E-06
-.2669E-13	-.2038E-11	-.1651E-13	-.1061E-04	.1534E-03	-.9590E-06
.1503E-13	-.6699E-14	.1054E-12	-.6381E-06	-.9590E-06	.3172E-03

a* b*/3
b*T d* 1/[gsi]

70.916	-7.354	.000	.000	.000	.000
-7.354	184.345	.000	.000	.000	.000
.000	.000	282.958	.000	.000	.000

.000	.000	.000	88.715	-8.912	-.536
.000	.000	.000	-8.912	128.857	-.805
.000	.000	.000	-.536	-.805	266.357

LAMINATE ENGINEERING CONSTANTS

N O T E ! !

Applies only to SYMMETRIC laminates

Inplane constants

E1o = 14.1012 E2o = 5.4246 E6o = 3.5341 [msi]

alp1o = .0304 alp2o = .8263 alp6o = .00001/[deg F]*1E6
bet1o = .0000 bet2o = .0000 bet6o = .0000 [#/#]

nu21o = .1037 nu61o = .0000 nu62o = .0000
nu12o = .0399 nu16o = .0000 nu26o = .0000

Flexural constants

E1f = 11.2721 E2f = 7.7605 E6f = 3.7544 [msi]

nu21f = .1005 nu61f = -.0060 nu62f = -.0063
nu12f = .0692 nu16f = -.0020 nu26f = -.0030

Load Case No 1

eps1	eps2	eps6	k1	k2	k6
-.9126E-05	-.2479E-03	.5179E-11	.7395E-01	-.7429E-02	-.4466E-03

eps1o	eps2o	eps6o	eps1f	eps2f	eps6f *1E3
-.0091	-.2479	.0000	7.9862	-.8023	-.0482

N1	N2	N6	M1	M2	M6
.0000E+00	.0000E+00	.0000E+00	.7000E+03	.0000E+00	.0000E+00

sigma1o	sigma2o	sigma6o	sigma1f	sigma2f	sigma6f [ksi]
.00	.00	.00	90.02	.00	.00

Temperature difference -300.0 Moisture .0000

Ply strains in 1000:s microstrains

Ply No	eps-1	eps-2	eps-6	eps-x	eps-y	eps-s
36 Top	7.9770	-1.0502	-.0482	7.9770	-1.0502	-.0482
36 Bot	7.5334	-1.0056	-.0456	7.5334	-1.0056	-.0456
35 Top	7.5334	-1.0056	-.0456	7.5334	-1.0056	-.0456
35 Bot	7.0897	-.9610	-.0429	7.0897	-.9610	-.0429
34 Top	7.0897	-.9610	-.0429	3.0429	3.0858	-8.0507
34 Bot	6.6460	-.9165	-.0402	2.8447	2.8849	-7.5625
33 Top	6.6460	-.9165	-.0402	2.8849	2.8447	7.5625
33 Bot	6.2023	-.8719	-.0375	2.6840	2.6465	7.0742
32 Top	6.2023	-.8719	-.0375	-.8719	6.2023	.0375
32 Bot	5.7587	-.8273	-.0348	-.8273	5.7587	.0348
31 Top	5.7587	-.8273	-.0348	-.8273	5.7587	.0348
31 Bot	5.3150	-.7828	-.0322	-.7828	5.3150	.0322
30 Top	5.3150	-.7828	-.0322	-.7828	5.3150	.0322
30 Bot	4.8713	-.7382	-.0295	-.7382	4.8713	.0295
29 Top	4.8713	-.7382	-.0295	2.0813	2.0518	5.6095
29 Bot	4.4276	-.6936	-.0268	1.8804	1.8536	5.1212

28 Top	4.4276	-.6936	-.0268	1.8536	1.8804	-5.1212
28 Bot	3.9840	-.6490	-.0241	1.6554	1.6795	-4.6330
27 Top	3.9840	-.6490	-.0241	3.9840	-.6490	-.0241
27 Bot	3.5403	-.6045	-.0214	3.5403	-.6045	-.0214
26 Top	3.5403	-.6045	-.0214	3.5403	-.6045	-.0214
26 Bot	3.0966	-.5599	-.0188	3.0966	-.5599	-.0188
25 Top	3.0966	-.5599	-.0188	3.0966	-.5599	-.0188
25 Bot	2.6529	-.5153	-.0161	2.6529	-.5153	-.0161
24 Top	2.6529	-.5153	-.0161	2.6529	-.5153	-.0161
24 Bot	2.2093	-.4708	-.0134	2.2093	-.4708	-.0134
23 Top	2.2093	-.4708	-.0134	2.2093	-.4708	-.0134
23 Bot	1.7656	-.4262	-.0107	1.7656	-.4262	-.0107
22 Top	1.7656	-.4262	-.0107	1.7656	-.4262	-.0107
22 Bot	1.3219	-.3816	-.0080	1.3219	-.3816	-.0080
21 Top	1.3219	-.3816	-.0080	1.3219	-.3816	-.0080
21 Bot	.8782	-.3370	-.0054	.8782	-.3370	-.0054
20 Top	.8782	-.3370	-.0054	.8782	-.3370	-.0054
20 Bot	.4346	-.2925	-.0027	.4346	-.2925	-.0027
19 Top	.4346	-.2925	-.0027	.4346	-.2925	-.0027
19 Bot	-.0091	-.2479	.0000	-.0091	-.2479	.0000
18 Top	-.0091	-.2479	.0000	-.0091	-.2479	.0000
18 Bot	-.4528	-.2033	.0027	-.4528	-.2033	.0027
17 Top	-.4528	-.2033	.0027	-.4528	-.2033	.0027
17 Bot	-.8965	-.1588	.0054	-.8965	-.1588	.0054
16 Top	-.8965	-.1588	.0054	-.8965	-.1588	.0054
16 Bot	-1.3402	-.1142	.0080	-1.3402	-.1142	.0080
15 Top	-1.3402	-.1142	.0080	-1.3402	-.1142	.0080
15 Bot	-1.7838	-.0696	.0107	-1.7838	-.0696	.0107
14 Top	-1.7838	-.0696	.0107	-1.7838	-.0696	.0107
14 Bot	-2.2275	-.0250	.0134	-2.2275	-.0250	.0134
13 Top	-2.2275	-.0250	.0134	-2.2275	-.0250	.0134
13 Bot	-2.6712	.0195	.0161	-2.6712	.0195	.0161
12 Top	-2.6712	.0195	.0161	-2.6712	.0195	.0161
12 Bot	-3.1149	.0641	.0188	-3.1149	.0641	.0188
11 Top	-3.1149	.0641	.0188	-3.1149	.0641	.0188
11 Bot	-3.5585	.1087	.0214	-3.5585	.1087	.0214
10 Top	-3.5585	.1087	.0214	-3.5585	.1087	.0214
10 Bot	-4.0022	.1532	.0241	-4.0022	.1532	.0241
9 Top	-4.0022	.1532	.0241	-1.9124	-1.9365	4.1554
9 Bot	-4.4459	.1978	.0268	-2.1106	-2.1374	4.6437
8 Top	-4.4459	.1978	.0268	-2.1374	-2.1106	-4.6437
8 Bot	-4.8896	.2424	.0295	-2.3383	-2.3088	-5.1319
7 Top	-4.8896	.2424	.0295	.2424	-4.8896	-.0295
7 Bot	-5.3332	.2870	.0322	.2870	-5.3332	-.0322
6 Top	-5.3332	.2870	.0322	.2870	-5.3332	-.0322

6 Bot	-5.7769	.3315	.0348	.3315	-5.7769	-.0348
5 Top	-5.7769	.3315	.0348	.3315	-5.7769	-.0348
5 Bot	-6.2206	.3761	.0375	.3761	-6.2206	-.0375
4 Top	-6.2206	.3761	.0375	-2.9410	-2.9035	-6.5967
4 Bot	-6.6643	.4207	.0402	-3.1419	-3.1017	-7.0849
3 Top	-6.6643	.4207	.0402	-3.1017	-3.1419	7.0849
3 Bot	-7.1079	.4652	.0429	-3.2999	-3.3428	7.5732
2 Top	-7.1079	.4652	.0429	-7.1079	.4652	.0429
2 Bot	-7.5516	.5098	.0456	-7.5516	.5098	.0456
1 Top	-7.5516	.5098	.0456	-7.5516	.5098	.0456
1 Bot	-7.9953	.5544	.0482	-7.9953	.5544	.0482

Ply stresses in ksi

Ply No	sigma-1	sigma-2	sigma-6	sigma-x	sigma-y	sigma-s
36 Top	159.31	2.62	-.15	159.31	2.62	-.15
36 Bot	150.42	2.58	-.14	150.42	2.58	-.14
35 Top	150.42	2.58	-.14	150.42	2.58	-.14
35 Bot	141.54	2.54	-.13	141.54	2.54	-.13
34 Top	57.33	7.42	28.60	60.97	3.78	-24.96
34 Bot	53.76	6.87	26.65	56.97	3.66	-23.44
33 Top	54.16	7.27	-27.06	57.77	3.65	23.44
33 Bot	50.56	6.70	-25.09	53.72	3.54	21.93
32 Top	4.62	-17.07	-.12	-17.07	4.62	.12
32 Bot	4.44	-16.24	-.11	-16.24	4.44	.11
31 Top	4.44	-16.24	-.11	-16.24	4.44	.11
31 Bot	4.25	-15.40	-.10	-15.40	4.25	.10
30 Top	4.25	-15.40	-.10	-15.40	4.25	.10
30 Bot	4.06	-14.57	-.09	-14.57	4.06	.09
29 Top	39.77	4.99	-19.18	41.57	3.20	17.39
29 Bot	36.18	4.43	-17.21	37.51	3.09	15.88
28 Top	35.91	4.16	16.94	36.98	3.10	-15.88
28 Bot	32.35	3.62	15.00	32.98	2.98	-14.36
27 Top	79.34	2.27	-.07	79.34	2.27	-.07
27 Bot	70.46	2.23	-.07	70.46	2.23	-.07
26 Top	70.46	2.23	-.07	70.46	2.23	-.07
26 Bot	61.57	2.20	-.06	61.57	2.20	-.06
25 Top	61.57	2.20	-.06	61.57	2.20	-.06
25 Bot	52.69	2.16	-.05	52.69	2.16	-.05
24 Top	52.69	2.16	-.05	52.69	2.16	-.05
24 Bot	43.80	2.12	-.04	43.80	2.12	-.04
23 Top	43.80	2.12	-.04	43.80	2.12	-.04
23 Bot	34.92	2.08	-.03	34.92	2.08	-.03
22 Top	34.92	2.08	-.03	34.92	2.08	-.03

22 Bot	26.03	2.04	-.02	26.03	2.04	-.02
21 Top	26.03	2.04	-.02	26.03	2.04	-.02
21 Bot	17.15	2.00	-.02	17.15	2.00	-.02
20 Top	17.15	2.00	-.02	17.15	2.00	-.02
20 Bot	8.26	1.96	-.01	8.26	1.96	-.01
19 Top	8.26	1.96	-.01	8.26	1.96	-.01
19 Bot	-.62	1.93	.00	-.62	1.93	.00
18 Top	-.62	1.93	.00	-.62	1.93	.00
18 Bot	-9.51	1.89	.01	-9.51	1.89	.01
17 Top	-9.51	1.89	.01	-9.51	1.89	.01
17 Bot	-18.40	1.85	.02	-18.40	1.85	.02
16 Top	-18.40	1.85	.02	-18.40	1.85	.02
16 Bot	-27.28	1.81	.02	-27.28	1.81	.02
15 Top	-27.28	1.81	.02	-27.28	1.81	.02
15 Bot	-36.17	1.77	.03	-36.17	1.77	.03
14 Top	-36.17	1.77	.03	-36.17	1.77	.03
14 Bot	-45.05	1.73	.04	-45.05	1.73	.04
13 Top	-45.05	1.73	.04	-45.05	1.73	.04
13 Bot	-53.94	1.69	.05	-53.94	1.69	.05
12 Top	-53.94	1.69	.05	-53.94	1.69	.05
12 Bot	-62.82	1.66	.06	-62.82	1.66	.06
11 Top	-62.82	1.66	.06	-62.82	1.66	.06
11 Bot	-71.71	1.62	.07	-71.71	1.62	.07
10 Top	-71.71	1.62	.07	-71.71	1.62	.07
10 Bot	-80.59	1.58	.07	-80.59	1.58	.07
9 Top	-31.90	-6.14	-19.96	-38.99	.94	12.88
9 Bot	-35.47	-6.68	-21.91	-42.98	.83	14.40
8 Top	-35.74	-6.95	22.18	-43.52	.84	-14.40
8 Bot	-39.33	-7.51	24.15	-47.57	.72	-15.91
7 Top	-.07	3.81	.09	3.81	-.07	-.09
7 Bot	-.25	4.64	.10	4.64	-.25	-.10
6 Top	-.25	4.64	.10	4.64	-.25	-.10
6 Bot	-.44	5.48	.11	5.48	-.44	-.11
5 Top	-.44	5.48	.11	5.48	-.44	-.11
5 Bot	-.63	6.31	.12	6.31	-.63	-.12
4 Top	-50.12	-9.22	30.05	-59.72	.38	-20.45
4 Bot	-53.72	-9.79	32.02	-63.78	.27	-21.96
3 Top	-53.32	-9.40	-31.62	-62.98	.26	21.96
3 Bot	-56.89	-9.94	-33.56	-66.97	.15	23.48
2 Top	-142.79	1.31	.13	-142.79	1.31	.13
2 Bot	-151.67	1.27	.14	-151.67	1.27	.14
1 Top	-151.67	1.27	.14	-151.67	1.27	.14
1 Bot	-160.56	1.23	.15	-160.56	1.23	.15

Load Case No 1; Quadratic Failure Criterion

Ply	Angle	Matr	h*1000	R-int/t	R-int/b	R-deg/t	R-deg/b
36	.0	12	6.0	1.97	2.09	1.72	1.82
35	.0	12	6.0	2.09	2.22	1.82	1.94
34	45.0	12	6.0	.893	.952	3.38	3.60
33	-45.0	12	6.0	.953	1.02	3.56	3.82
32	90.0	12	6.0	2.86	3.08	3.85	4.14
31	90.0	12	6.0	3.08	3.34	4.14	4.49
30	90.0	12	6.0	3.34	3.64	4.49	4.90
29	-45.0	12	6.0	1.30	1.43	4.86	5.35
28	45.0	12	6.0	1.43	1.59	5.40	6.00
27	.0	12	6.0	3.94	4.43	3.44	3.87
26	.0	12	6.0	4.43	5.06	3.87	4.42
25	.0	12	6.0	5.06	5.91	4.42	5.16
24	.0	12	6.0	5.91	7.09	5.16	6.19
23	.0	12	6.0	7.09	8.86	6.19	7.74
22	.0	12	6.0	8.86	11.8	7.74	10.3
21	.0	12	6.0	11.8	17.7	10.3	15.5
20	.0	12	6.0	17.7	35.4	15.5	31.0
19	.0	12	6.0	35.4	.979E+07	31.0	.699E+07
18	.0	12	6.0	.979E+07	16.5	.699E+07	13.3
17	.0	12	6.0	16.5	8.23	13.3	6.67
16	.0	12	6.0	8.23	5.48	6.67	4.45
15	.0	12	6.0	5.48	4.11	4.45	3.34
14	.0	12	6.0	4.11	3.29	3.34	2.67
13	.0	12	6.0	3.29	2.74	2.67	2.22
12	.0	12	6.0	2.74	2.35	2.22	1.91
11	.0	12	6.0	2.35	2.06	1.91	1.67
10	.0	12	6.0	2.06	1.83	1.67	1.48
9	45.0	12	6.0	1.51	1.36	3.28	2.95
8	-45.0	12	6.0	1.36	1.23	2.90	2.63
7	90.0	12	6.0	12.5	11.4	13.4	12.3
6	90.0	12	6.0	11.4	10.6	12.3	11.3
5	90.0	12	6.0	10.6	9.81	11.3	10.5
4	-45.0	12	6.0	.969	.904	2.07	1.93
3	45.0	12	6.0	.907	.850	1.97	1.84
2	.0	12	6.0	1.03	.968	.834	.785
1	.0	12	6.0	.968	.914	.785	.742

Loadcase	FPF	Ultimate	Safety	Limit*	Limit
1	.850	.850	1.00	.850	.850

APPENDIX B: GENLAM Temperature Differential Calculations

Results from GENLAM calculations for the hybrid steel/ composite bar bonded without an adhesive with a temperature differential of -400°F

Laminate stiffness matrix

.5480E+08	.1234E+08	.0000E+00	-.1776E-01	.6771E-01	.0000E+00
.1234E+08	.4226E+08	.0000E+00	.6771E-01	-.1776E-01	0000E+00
.0000E+00	.0000E+00	.1670E+08	.000E+00	.000E+00	-.1190E+00

-.1776E-01	.6771E-01	.0000E+00	.1907E+08	.5442E+07	.0000E+00
.6771E-01	-.1776E-01	.0000E+00	.5442E+07	.1864E+08	0000E+00
.0000E+00	.0000E+00	-.1190E+00	.0000E+00	.000E+00	6599E+07

A* B*
3B* D* [msi]

28.544	6.428	.000	.000	.000	.000
6.428	22.010	.000	.000	.000	.000
.000	.000	8.700	.000	.000	.000

.000	.000	.000	32.324	9.227	.000
.000	.000	.000	9.227	31.598	.000
.000	.000	.000	.000	.000	11.189

Laminate compliance matrix

.1953E-07	-.5704E-08	.0000E+00	.6573E-16	-.9558E-16	.0000E+00
-.5704E-08	.2533E-07	.0000E+00	-.1179E-15	.7928E-16	.0000E+00
.0000E+00	.0000E+00	.5987E-07	.0000E+00	.000E+00	.1079E-14

.6573E-16	-.1179E-15	.0000E+00	.5722E-07	-.1671E-07	.0000E+00
-.9558E-16	.7928E-16	.0000E+00	-.1671E-07	.5854E-07	.0000E+00
.0000E+00	.0000E+00	.1079E-14	.0000E+00	.000E+00	.1515E-06

a* b*/3
b*T d* 1/[gsi]

37.500	-10.952	.000	.000	.000	.000
-10.952	48.633	.000	.000	.000	.000
.000	.000	114.943	.000	.000	.000
.000	.000	.000	33.750	-9.855	.000
.000	.000	.000	-9.855	34.526	.000
.000	.000	.000	.000	.000	89.374

Think Composites's GENLAM V

LAMINATE ENGINEERING CONSTANTS

N O T E ! !

Applies only to SYMMETRIC laminates

Inplane constants

E1o = 26.6667 E2o = 20.5620 E6o = 8.7000 [msi]

alp1o = 4.4578 alp2o = 6.5016 alp6o = .00001/[deg F]*1E6
bet1o = .0000 bet2o = .0000 bet6o = .0000 [#/#]

nu21o = .2921 nu61o = .0000 nu62o = .0000
nu12o = .2252 nu16o = .0000 nu26o = .0000

Flexural constants

E1f = 29.6296 E2f = 28.9641 E6f = 11.1889 [msi]

nu21f = .2920 nu61f = .0000 nu62f = .0000
nu12f = .2854 nu16f = .0000 nu26f = .0000

Load Case No 1

eps1	eps2	eps6	k1	k2	k6
-.1783E-02	-.2601E-02	.000E+00	-.4859E-10	-.5547E-10	.0000E+00

eps1o	eps2o	eps6o	eps1f	eps2f	eps6f *1E3
-1.7831	-2.6006	.0000	.0000	.0000	.0000

N1	N2	N6	M1	M2	M6
.0000E+00	.0000E+00	.000E+00	.0000E+00	.0000E+00	.0000E+00

sigma1o	sigma2o	sigma6o	sigma1f	sigma2f	sigma6f [ksi]
.00	.00	.00	.00	.00	.00

Temperature difference -400.0 Moisture .0000

Think Composites's GENLAM V

Ply strains in 1000:s microstrains

Ply No	eps-1	eps-2	eps-6	eps-x	eps-y	eps-s
4 Top	-1.7831	-2.6006	.0000	-1.7831	-2.6006	.0000
4 Bot	-1.7831	-2.6006	.0000	-1.7831	-2.6006	.0000
3 Top	-1.7831	-2.6006	.0000	-1.7831	-2.6006	.0000
3 Bot	-1.7831	-2.6006	.0000	-1.7831	-2.6006	.0000
2 Top	-1.7831	-2.6006	.0000	-1.7831	-2.6006	.0000
2 Bot	-1.7831	-2.6006	.0000	-1.7831	-2.6006	.0000
1 Top	-1.7831	-2.6006	.0000	-1.7831	-2.6006	.0000
1 Bot	-1.7831	-2.6006	.0000	-1.7831	-2.6006	.0000

Ply stresses in ksi

Ply No	sigma-1	sigma-2	sigma-6	sigma-x	sigma-y	sigma-s
4 Top	18.31	-.67	.00	18.31	-.67	.00
4 Bot	18.31	-.67	.00	18.31	-.67	.00
3 Top	-36.62	1.35	.00	-36.62	1.35	.00
3 Bot	-36.62	1.35	.00	-36.62	1.35	.00
2 Top	-36.62	1.35	.00	-36.62	1.35	.00
2 Bot	-36.62	1.35	.00	-36.62	1.35	.00
1 Top	18.31	-.67	.00	18.31	-.67	.00
1 Bot	18.31	-.67	.00	18.31	-.67	.00